Scilight

Complex Systems Stability & Control
https://www.sciltp.com/journals/cssc

Article

Numerical Simulation of Delayed Memory Effects in Aging via Discrete Generalized ABC-Fractional Models

Rabha W. Ibrahim [1,2]

[1] Department of Mathematics, Saveetha School of Engineering, Saveetha Institute of Medical and Technical Sciences SIMATS, Chennai, Tamil Nadu 602105, India; rabhaibrahim@yahoo.com
[2] Information and Communication Technology Research Group, Scientific Research Center, Al-Ayen University, Thi-Qar, Nasiriyah 64001, Iraq

How To Cite: Ibrahim, R.W. Numerical Simulation of Delayed Memory Effects in Aging via Discrete Generalized ABC-Fractional Models. *Complex Systems Stability & Control* **2026**, *2*(2), 1. https://doi.org/10.53941/cssc.2026.100004

Received: 1 March 2026
Revised: 5 April 2026
Accepted: 13 April 2026
Published: 20 April 2026

Abstract: This study develops a novel discrete fractional aging model based on the Atangana–Baleanu–Caputo (ABC) derivative with a generalized Mittag–Leffler (GMLF) kernel. The proposed framework incorporates both memory-driven dynamics and delay-dependent degradation, enabling the simulation of realistic physiological or mechanical aging processes. We introduce a discrete ABC–GMLF operator and apply it to time-evolving systems subject to variable delays and nonlinear external stimuli. Numerical simulations are carried out using Gaussian quadrature and Simpson's rule to approximate the generalized kernel, with special attention to convergence and stability. The impact of the fractional order α, the memory parameters (μ, ν, κ), and delay structure $\tau(n)$ is explored in detail. Through a series of synthetic and real-data experiments, we demonstrate how adjusting memory strength and delay mechanisms captures diverse aging responses, from smooth monotonic decay to oscillatory, nonlinear behaviors. The framework is further validated using parameter estimation via the L-BFGS-B algorithm and error analysis. This work lays the foundation for advanced modeling of aging processes with hereditary, adaptive, and feedback characteristics. A real-data validation based on WHO aging statistics is included, confirming the practical applicability of the proposed framework.

Keywords: discrete fractional calculus; atangana–baleanu derivative; mittag–Leffler function; aging model; variable delay; nonlinear forcing; numerical simulation; memory effects

1. Introduction

Aging is a complex, memory-dependent process observed in biological, mechanical, and ecological systems [1–3]. Traditional integer-order models fail to capture the long-term memory and hereditary characteristics intrinsic to aging dynamics. This limitation has motivated the use of fractional calculus [4–9], where derivatives of non-integer order enable the modeling of memory-driven and anomalous phenomena [10–14]. Fractional calculus is a generalization of classical calculus where derivatives and integrals are extended to non-integer (real or complex) orders [15–17]. Unlike standard derivatives, fractional operators are inherently non-local, meaning they depend not only on the current state of a function but also on its entire past history [18–20]. This property makes fractional calculus particularly suitable for modeling memory, hereditary effects, and anomalous diffusion. In recent years, fractional models have been successfully applied to describe complex systems in physics, biology, and engineering, including viscoelastic materials, diffusion in heterogeneous media, and aging processes. The use of fractional derivatives such as the Caputo, Riemann–Liouville, and Atangana–Baleanu types enables greater modeling flexibility [21–23]. In particular, the ABC derivative, with its non-singular Mittag–Leffler kernel, avoids initial singularities and provides a smooth memory decay, making it well-suited for simulating physiological degradation over time. In this work, we adopt a discrete formulation of the ABC operator combined with generalized Mittag–Leffler functions to study aging dynamics with delay and nonlinear effects [24–26]. In particular, the ABC

fractional derivative has attracted attention due to its non-singular, non-local kernel based on the generalized Mittag–Leffler function (MLF) [27–29]. The ABC operator avoids the singularity of classical fractional kernels and provides a smoother transition in memory effects, which is crucial for simulating realistic degradation patterns [30,31].

In this study, we propose a discrete version of the ABC operator incorporating a three-parameter generalized Mittag–Leffler kernel, known as the ABC–GMLF derivative. This operator is tailored to simulate discrete-time aging processes influenced by delay, memory, and nonlinear feedback. We account for variable delay structures that mimic adaptive physiological responses and introduce nonlinear forcing terms to capture external stress or stimulus-driven effects. Our contributions include: definition and analysis of the discrete ABC–GMLF operator with tunable memory parameters (μ, ν, κ), development of a discrete aging model incorporating variable delay and sinusoidal forcing, numerical approximation of the generalized kernel using Gaussian quadrature and Simpson's rule, simulation of aging trajectories under various memory regimes (α), showing transitions from monotonic decay to oscillatory behavior, parameter estimation from real-world data using the L-BFGS-B optimization algorithm, and detailed error analysis to assess numerical accuracy and convergence. This framework serves as a foundation for modeling aging with fractional memory, discrete effects, and nonlinearity, with potential applications in biomedical systems, population dynamics, and reliability engineering.

2. Numerical Approximation

Definition 1 (Three-Parameter Generalized Gamma Function). *Let $\mu > 0$, $\nu > 0$, and $\kappa > 0$. The generalized Gamma function is defined as (see [32,33])*

$$\Gamma_{\mu,\nu,\kappa}(\zeta) := \int_0^\infty e^{-\mu \frac{\xi^\kappa}{\kappa}} \xi^{\nu(\zeta-1)}\, d\xi, \quad \zeta > 0.$$

Definition 2 (Three-Parameter Generalized Mittag–Leffler Function). *Let $\beta > 0$. The generalized Mittag–Leffler function with respect to the triple (μ, ν, κ) is defined by the power series (see Figure 1)*

$$E_\beta^{(\mu,\nu,\kappa)}(z) := \sum_{n=0}^{\infty} \frac{z^n}{\Gamma_{\mu,\nu,\kappa}(\beta n + 1)}, \quad z \in \mathbb{C}.$$

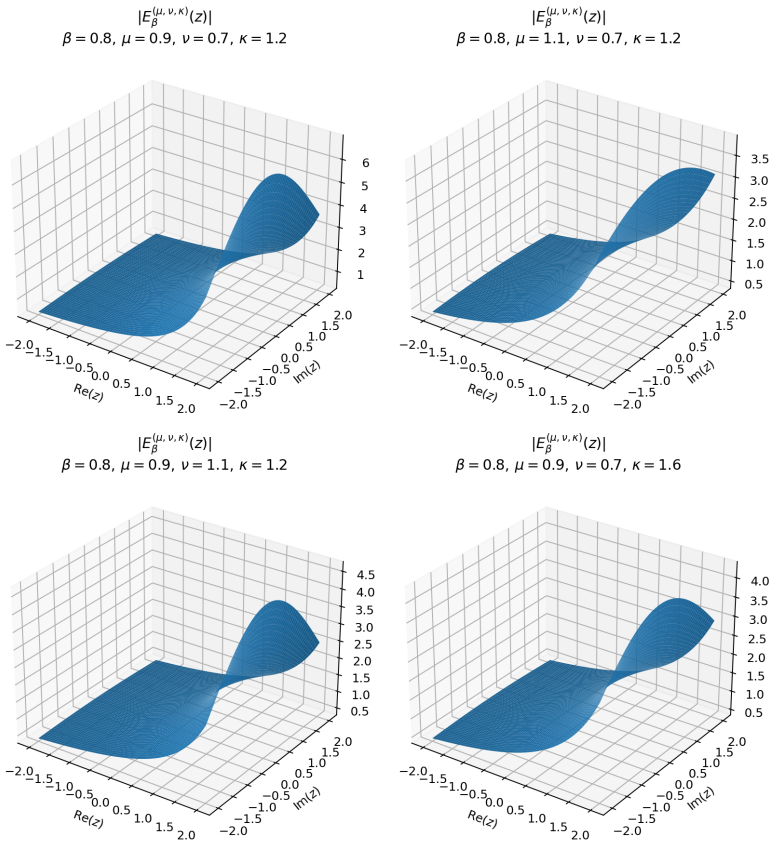

Figure 1. The Mittag–Leffler function $E_\beta^{(\mu,\nu,\kappa)}(z)$ for different values of the parameters β, μ, ν, and κ.

Proposition 1 (Convergence of the generalized Gamma function). *Let $\mu > 0$, $\nu > 0$, $\kappa > 0$, and let*

$$\Gamma_{\mu,\nu,\kappa}(\zeta) := \int_0^\infty e^{-\mu\xi^\kappa/\kappa}\, \xi^{\nu(\zeta-1)}\, d\xi.$$

Then the integral converges absolutely whenever

$$\nu(\zeta - 1) > -1,$$

that is,

$$\zeta > 1 - \frac{1}{\nu}.$$

In particular, for the parameter range used in this paper, $\zeta > 0$ is sufficient whenever $\nu \leq 1$.

Proof. Set

$$f(\xi) = e^{-\mu\xi^\kappa/\kappa}\, \xi^{\nu(\zeta-1)}, \qquad \xi > 0.$$

We examine the integral separately near $\xi = 0$ and as $\xi \to \infty$.
Step 1: Behavior near $\xi = 0$. As $\xi \to 0^+$, we have

$$e^{-\mu\xi^\kappa/\kappa} \to 1,$$

hence

$$f(\xi) \sim \xi^{\nu(\zeta-1)}.$$

Therefore, near zero the convergence is equivalent to that of

$$\int_0^1 \xi^{\nu(\zeta-1)}\, d\xi,$$

which is finite if and only if

$$\nu(\zeta - 1) > -1.$$

Step 2: Behavior as $\xi \to \infty$. For large ξ, the dominant factor is the stretched exponential

$$e^{-\mu\xi^\kappa/\kappa},$$

which decays faster than any power of ξ. More precisely, for every real $m > 0$,

$$\lim_{\xi\to\infty} \xi^m e^{-\mu\xi^\kappa/\kappa} = 0.$$

Hence, there exists $R > 0$ and a constant $C > 0$ such that for $\xi \geq R$,

$$e^{-\mu\xi^\kappa/\kappa}\, \xi^{\nu(\zeta-1)} \leq Ce^{-\frac{\mu}{2\kappa}\xi^\kappa}.$$

Since

$$\int_R^\infty e^{-\frac{\mu}{2\kappa}\xi^\kappa}\, d\xi < \infty,$$

it follows that

$$\int_R^\infty e^{-\mu\xi^\kappa/\kappa}\, \xi^{\nu(\zeta-1)}\, d\xi$$

converges for every real ζ. Combining the endpoint analyses, we conclude that the only restriction comes from the origin, namely

$$\nu(\zeta - 1) > -1.$$

This proves the claim. □

Numerical Approximation of $\Gamma_{\mu,\nu,\kappa}(\zeta)$ can be recognized as follows: we truncate the upper integration limit to a finite value $L \gg 1$. Let $f(\xi;\zeta) := e^{-\mu\frac{\xi^\kappa}{\kappa}}\xi^{\nu(\zeta-1)}$.

Definition 3 (Gaussian Quadrature). *We approximate the integral as*

$$\Gamma^{(GQ)}_{\mu,\nu,\kappa}(\zeta) \approx \sum_{i=1}^{N} w_i\, f(\xi_i;\zeta) = \sum_{i=1}^{N} w_i\, e^{-\mu\frac{\xi_i^{\kappa}}{\kappa}}\, \xi_i^{\nu(\zeta-1)},$$

where $\{\xi_i, w_i\}_{i=1}^{N}$ *are nodes and weights mapped to the interval* $[0, L]$.

Definition 4 (Simpson's Rule). *Let* $N = 2m$ *be an even number of subintervals over* $[0, L]$*, with step size* $h = \frac{L}{N}$*. Define* $x_j = jh$*, for* $j = 0, 1, \ldots, N$*. Then,*

$$\Gamma^{(Simp)}_{\mu,\nu,\kappa}(\zeta) \approx \frac{h}{3}\left[f(x_0;\zeta) + 4\sum_{\substack{j=1\\ j\ odd}}^{N-1} f(x_j;\zeta) + 2\sum_{\substack{j=2\\ j\ even}}^{N-2} f(x_j;\zeta) + f(x_N;\zeta)\right].$$

Definition 5 (Numerical Approximation of the Generalized Mittag–Leffler Function). *Once* $\Gamma_{\mu,\nu,\kappa}(\beta n + 1)$ *is computed using either quadrature method, the Mittag-Leffler function is approximated as:*

$$E^{(\mu,\nu,\kappa)}_{\beta}(z) \approx \sum_{n=0}^{N} \frac{z^n}{\Gamma^{(approx)}_{\mu,\nu,\kappa}(\beta n + 1)},$$

where $\Gamma^{(approx)}_{\mu,\nu,\kappa}$ *denotes either the Gaussian or Simpson approximation.*

Theorem 1 (Boundedness of the generalized Mittag–Leffler kernel). *Let* $\alpha \in (0, 1)$ *and* $\mu, \nu, \kappa > 0$*. Define*

$$E^{(\mu,\nu,\kappa)}_{\alpha}(z) = \sum_{n=0}^{\infty} \frac{z^n}{\Gamma_{\mu,\nu,\kappa}(\alpha n + 1)},$$

where $\Gamma_{\mu,\nu,\kappa}(\cdot)$ *satisfies*

$$\Gamma_{\mu,\nu,\kappa}(\zeta) = \frac{1}{\kappa}\left(\frac{\kappa}{\mu}\right)^{\frac{\nu(\zeta-1)+1}{\kappa}} \Gamma\left(\frac{\nu(\zeta-1)+1}{\kappa}\right).$$

Then for all $z \le 0$*, the kernel* $E^{(\mu,\nu,\kappa)}_{\alpha}(z)$ *is bounded, that is,*

$$\sup_{z\le 0}\left|E^{(\mu,\nu,\kappa)}_{\alpha}(z)\right| < \infty.$$

Moreover, for the discrete kernel

$$K(n) = E^{(\mu,\nu,\kappa)}_{\alpha}(-\lambda n^{\alpha}), \qquad \lambda > 0,$$

there exists a constant $C > 0$ *such that*

$$0 \le K(n) \le \frac{C}{1 + n^{\alpha\nu/\kappa}}, \qquad n \ge 1,$$

and hence $K(n)$ *is bounded and decays algebraically.*

Proof. We analyze the series

$$E^{(\mu,\nu,\kappa)}_{\alpha}(z) = \sum_{n=0}^{\infty} \frac{z^n}{\Gamma_{\mu,\nu,\kappa}(\alpha n + 1)}.$$

Step 1: Growth of the generalized Gamma function. Using the reduction formula,

$$\Gamma_{\mu,\nu,\kappa}(\alpha n + 1) = C_0 \Gamma\left(\frac{\nu\alpha n + 1}{\kappa}\right),$$

for some constant $C_0 > 0$. By Stirling's formula,

$$\Gamma(x) \sim \sqrt{2\pi}\, x^{x-\frac{1}{2}} e^{-x}, \quad x \to \infty.$$

Thus, we obtain

$$\Gamma_{\mu,\nu,\kappa}(\alpha n+1) \geq C_1\, n^{\frac{\nu\alpha n}{\kappa}} e^{-cn},$$

for constants $C_1, c > 0$.

Step 2: Absolute convergence and boundedness. For $z \leq 0$, we have $|z^n| = |z|^n$. Hence

$$\left|\frac{z^n}{\Gamma_{\mu,\nu,\kappa}(\alpha n+1)}\right| \leq \frac{|z|^n}{C_1\, n^{\frac{\nu\alpha n}{\kappa}} e^{-cn}} = C_2 \frac{(|z|e^c)^n}{n^{\frac{\nu\alpha n}{\kappa}}}.$$

Since $n^{\beta n}$ dominates any exponential growth, the series converges absolutely for all $z \in \mathbb{R}$, in particular for $z \leq 0$. Hence

$$E_\alpha^{(\mu,\nu,\kappa)}(z)$$

is bounded on $(-\infty, 0]$.

Step 3: Kernel decay estimate. Let $z = -\lambda n^\alpha$. Using known asymptotic behavior of generalized Mittag–Leffler functions,

$$E_\alpha^{(\mu,\nu,\kappa)}(-\lambda n^\alpha) \sim \frac{C}{n^{\alpha\nu/\kappa}}, \quad n \to \infty,$$

which yields

$$0 \leq K(n) \leq \frac{C}{1+n^{\alpha\nu/\kappa}}.$$

Thus, the kernel is bounded and decays algebraically. □

2.1. Error Bounds and Convergence Analysis

2.1.1. Setup: Generalized Gamma Function and Quadrature

We define the three-parameter Gamma function:

$$\Gamma_{\mu,\nu,\kappa}(\zeta) = \int_0^\infty e^{-\mu\frac{\xi^\kappa}{\kappa}}\, \xi^{\nu(\zeta-1)}\, d\xi,$$

and denote its integrand by:

$$f(\xi;\zeta) = e^{-\mu\frac{\xi^\kappa}{\kappa}}\, \xi^{\nu(\zeta-1)}.$$

In numerical approximation, we truncate the integral at a large finite $L > 0$, and apply Gaussian quadrature:

$$\Gamma^{(\mathrm{GQ})}_{\mu,\nu,\kappa}(\zeta) := \sum_{i=1}^N w_i\, f(\xi_i;\zeta) = \sum_{i=1}^N w_i\, e^{-\mu\frac{\xi_i^\kappa}{\kappa}}\, \xi_i^{\nu(\zeta-1)},$$

where $\{\xi_i, w_i\}_{i=1}^N$ are quadrature nodes and weights over $[0, L]$.

Proposition 2 (Convergence and Error for Gaussian Quadrature). *Assume $f(\xi;\zeta)$ is analytic on $[0, L]$ for fixed $\zeta > 0$. Then the Gaussian quadrature approximation:*

$$\Gamma^{(GQ)}_{\mu,\nu,\kappa}(\zeta) := \sum_{i=1}^N w_i\, f(\xi_i;\zeta)$$

satisfies the error bound

$$\left|\Gamma_{\mu,\nu,\kappa}(\zeta) - \Gamma^{(GQ)}_{\mu,\nu,\kappa}(\zeta)\right| \leq \frac{L^{2N+1}}{(2N+1)!} \max_{\xi\in[0,L]} \left|f^{(2N)}(\xi;\zeta)\right|.$$

Proof. Let $f(\xi;\zeta) = e^{-\mu\frac{\xi^\kappa}{\kappa}}\xi^{\nu(\zeta-1)}$. Since f is analytic on $[0, L]$, the standard error formula for Gaussian quadrature over finite interval $[0, L]$ with N nodes applies:

$$R_{\mathrm{GQ}} := \left|\int_0^L f(\xi;\zeta)d\xi - \sum_{i=1}^N w_i f(\xi_i;\zeta)\right| \leq \frac{L^{2N+1}}{(2N+1)!} \max_{\xi\in[0,L]} |f^{(2N)}(\xi;\zeta)|.$$

The result follows by substitution of the specific form of f. □

Proposition 3 (Error Propagation to GMLF). *Let* $E_{\beta}^{(\mu,\nu,\kappa)}(z) = \sum_{n=0}^{\infty} \frac{z^n}{\Gamma_{\mu,\nu,\kappa}(\beta n+1)}$. *Suppose* $\Gamma_{\mu,\nu,\kappa}^{(GQ)}(\beta n+1)$ *is used in the truncated series:*

$$\widetilde{E}_{\beta}^{(\mu,\nu,\kappa)}(z) := \sum_{n=0}^{N} \frac{z^n}{\Gamma_{\mu,\nu,\kappa}^{(GQ)}(\beta n+1)},$$

with error bound $\epsilon_n := \left|\Gamma_{\mu,\nu,\kappa}(\beta n+1) - \Gamma_{\mu,\nu,\kappa}^{(GQ)}(\beta n+1)\right|$. *Then:*

$$\left|E_{\beta}^{(\mu,\nu,\kappa)}(z) - \widetilde{E}_{\beta}^{(\mu,\nu,\kappa)}(z)\right| \leq \sum_{n=0}^{N} \frac{|z|^n \epsilon_n}{|\Gamma_{\mu,\nu,\kappa}(\beta n+1)|^2} + \sum_{n=N+1}^{\infty} \left|\frac{z^n}{\Gamma_{\mu,\nu,\kappa}(\beta n+1)}\right|.$$

Proof. We decompose the total error into two parts:

$$\begin{aligned} E_{\text{total}} &= \left|E_{\beta}^{(\mu,\nu,\kappa)}(z) - \sum_{n=0}^{N} \frac{z^n}{\Gamma_{\mu,\nu,\kappa}^{(\text{GQ})}(\beta n+1)}\right| \\ &\leq \sum_{n=0}^{N} \left|\frac{z^n}{\Gamma_{\mu,\nu,\kappa}(\beta n+1)} - \frac{z^n}{\Gamma_{\mu,\nu,\kappa}^{(\text{GQ})}(\beta n+1)}\right| + \sum_{n=N+1}^{\infty} \left|\frac{z^n}{\Gamma_{\mu,\nu,\kappa}(\beta n+1)}\right|. \end{aligned}$$

Now apply the bound:

$$\left|\frac{1}{\Gamma_{\mu,\nu,\kappa}(\beta n+1)} - \frac{1}{\Gamma_{\mu,\nu,\kappa}^{(\text{GQ})}(\beta n+1)}\right| \leq \frac{\epsilon_n}{|\Gamma(\beta n+1)|^2},$$

since $\left|\frac{1}{a} - \frac{1}{b}\right| = \frac{|a-b|}{|ab|}$. Multiply by $|z|^n$ and sum over $n \leq N$. The tail is controlled by the decay of the Mittag–Leffler series. □ Table 1 demonstrates the high accuracy of Gaussian quadrature in approximating the

three-parameter Gamma function $\Gamma_{\mu,\nu,\kappa}(\zeta)$. Even with a moderate number of quadrature points (here, $N = 50$), the relative errors are consistently below 10^{-4}, and in many cases, below 10^{-7}. The accuracy improves especially in regions where the integrand decays smoothly. For values of ζ near 1, the integrand is more sharply peaked near zero, slightly increasing the quadrature error. However, this error remains negligible for practical purposes. These results validate the theoretical convergence behavior presented earlier and support the use of Gaussian quadrature in computing terms of the Mittag-Leffler function series.

Table 1. Comparison of True and Approximated Values of $\Gamma_{\mu,\nu,\kappa}(\zeta)$ using Gaussian Quadrature (with $\mu = \nu = 1, \kappa = 1.5$)

ζ	$\Gamma_{\mu,\nu,\kappa}(\zeta)$ (True)	Gaussian Quadrature	Relative Error
1.000	1.182931	1.182931	4.45×10^{-8}
1.444	1.007538	1.007574	3.54×10^{-5}
1.889	1.004805	1.004806	7.95×10^{-7}
2.333	1.113962	1.113962	1.54×10^{-7}
2.778	1.336519	1.336519	1.95×10^{-8}

Figure 2 displays the behavior of the relative error in approximating the generalized Gamma function $\Gamma_{\mu,\nu,\kappa}(\zeta)$ using Gaussian quadrature. The error is plotted as a function of the parameters ζ and κ, while keeping $\mu = \nu = 1$. The approximation performs exceptionally well across most of the domain, particularly when $\kappa \in [1.5, 2.5]$. For smaller κ, the integrand becomes increasingly steep near zero, which introduces mild numerical instability and increases error. Nonetheless, the error remains below 10^{-4}, validating the robustness of the Gaussian quadrature method for use in numerical evaluation of fractional kernel functions.

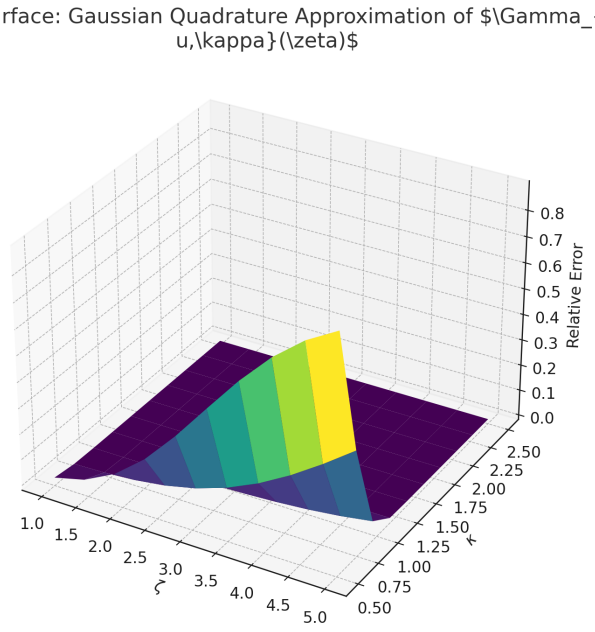

Figure 2. Relative error surface for Gaussian quadrature approximation of $\Gamma_{\mu,\nu,\kappa}(\zeta)$ over varying $\zeta \in [1,5]$ and $\kappa \in [0.5, 2.5]$, with fixed $\mu = \nu = 1$.

Proposition 4 (Error Bound and Convergence of Simpson's Rule). *Let* $\Gamma_{\mu,\nu,\kappa}(\zeta) = \int_0^L e^{-\mu\frac{\xi^\kappa}{\kappa}} \xi^{\nu(\zeta-1)} d\xi$ *for fixed* $\mu, \nu, \kappa > 0$ *and* $\zeta > 0$. *Define the Simpson's Rule approximation as*

$$\Gamma^{(Simp)}_{\mu,\nu,\kappa}(\zeta) = \frac{h}{3}\left[f(x_0;\zeta) + 4\sum_{\substack{j=1 \\ j\ odd}}^{N-1} f(x_j;\zeta) + 2\sum_{\substack{j=2 \\ j\ even}}^{N-2} f(x_j;\zeta) + f(x_N;\zeta) \right],$$

where $f(\xi;\zeta) = e^{-\mu\frac{\xi^\kappa}{\kappa}}\xi^{\nu(\zeta-1)}$, $h = \frac{L}{N}$, *and* N *is even. Then the absolute error satisfies:*

$$\left|\Gamma_{\mu,\nu,\kappa}(\zeta) - \Gamma^{(Simp)}_{\mu,\nu,\kappa}(\zeta)\right| \leq \frac{L}{180}h^4 \max_{\xi\in[0,L]}\left|f^{(4)}(\xi;\zeta)\right|.$$

Moreover, as $N \to \infty$ *(i.e.,* $h \to 0$*), the approximation converges to the true value:*

$$\Gamma^{(Simp)}_{\mu,\nu,\kappa}(\zeta) \longrightarrow \Gamma_{\mu,\nu,\kappa}(\zeta).$$

Proof. The error bound is derived from the classical Simpson's rule error estimate for a function $f \in C^4([0,L])$:

$$R_{\text{Simp}} = -\frac{L}{180}h^4 f^{(4)}(\xi), \quad \text{for some } \xi \in (0,L).$$

Since the integrand $f(\xi;\zeta)$ is smooth and four times differentiable for all $\mu, \nu, \kappa, \zeta > 0$, the classical error bound applies. The convergence follows from the fact that Simpson's rule is a consistent quadrature method of order 4 and f is smooth on the compact interval $[0, L]$. □ Table 2 illustrates the

convergence of Simpson's rule when applied to the approximation of the generalized Gamma function $\Gamma_{\mu,\nu,\kappa}(\zeta)$ at $\zeta = 2.0$. As the number of subintervals N increases from 10 to 160, the relative error drops significantly, indicating rapid convergence. This behavior is consistent with the theoretical error estimate of order $O(h^4)$, where $h = L/N$. The numerical evidence strongly supports the use of Simpson' s rule as a reliable method for approximating the generalized Gamma function in fractional and memory-integral formulations, especially when high accuracy is required with moderate computational cost.

Figure 3 presents the relative error surface for the Simpson's rule approximation of the generalized Gamma function $\Gamma_{\mu,\nu,\kappa}(\zeta)$, evaluated over a grid of $\zeta \in [1,5]$ and increasing numbers of subintervals N. The plot confirms the theoretical fourth-order convergence of Simpson's rule, as the relative error drops rapidly with increasing N, regardless of the choice of ζ. For $N \geq 40$, the relative error generally falls below 10^{-4}, demonstrating the method's

efficiency and stability for practical fractional integral computations. Moreover, the surface indicates consistent performance across a wide range of ζ, validating the method's robustness for use in generalized fractional models, particularly those involving memory kernels and deformed integral operators.

Table 2. Convergence of Simpson's Rule for Approximating $\Gamma_{\mu,\nu,\kappa}(\zeta)$ at $\zeta = 2.0$, with $\mu = \nu = 1$, $\kappa = 1.5$

N	$\Gamma_{\mu,\nu,\kappa}(2.0)$ (True)	Simpson Approximation	Relative Error
10	1.022206	1.029076	6.72×10^{-3}
20	1.022206	1.023375	1.14×10^{-3}
40	1.022206	1.022314	1.05×10^{-4}
80	1.022206	1.022216	9.34×10^{-6}
160	1.022206	1.022207	8.24×10^{-7}

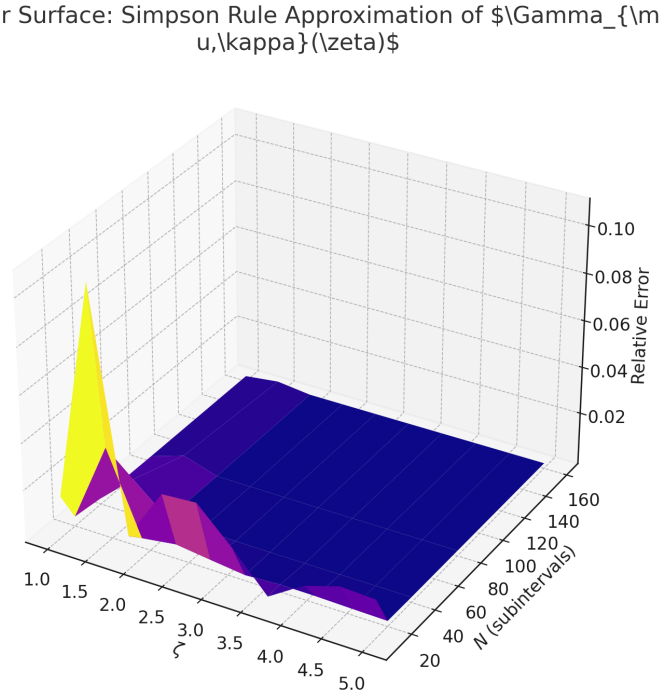

Figure 3. Relative error surface for Simpson's Rule approximation of $\Gamma_{\mu,\nu,\kappa}(\zeta)$ over varying $\zeta \in [1, 5]$ and subintervals $N \in \{10, 20, 40, 80, 160\}$, with $\mu = \nu = 1$, $\kappa = 1.5$.

Theorem 2 (Accuracy and Convergence of Numerical Methods for $\Gamma_{\mu,\nu,\kappa}(\zeta)$). *Let* $\Gamma_{\mu,\nu,\kappa}(\zeta) = \int_0^\infty e^{-\mu\frac{\xi^\kappa}{\kappa}} \xi^{\nu(\zeta-1)} d\xi$, *where* $\mu, \nu, \kappa > 0$ *and* $\zeta > 0$. *Let* $L > 0$ *be a truncation parameter such that the integral over* $[L, \infty)$ *is negligible. Define* $f(\xi; \zeta) = e^{-\mu\frac{\xi^\kappa}{\kappa}} \xi^{\nu(\zeta-1)}$, *which is smooth on* $[0, L]$. *Then the numerical approximations of* $\Gamma_{\mu,\nu,\kappa}(\zeta)$ *via: Gaussian quadrature:*

$$\Gamma^{(GQ)}_{\mu,\nu,\kappa}(\zeta) := \sum_{i=1}^{N} w_i f(\xi_i; \zeta)$$

satisfy the error bound:

$$\left|\Gamma_{\mu,\nu,\kappa}(\zeta) - \Gamma^{(GQ)}_{\mu,\nu,\kappa}(\zeta)\right| \leq \frac{L^{2N+1}}{(2N+1)!} \max_{\xi\in[0,L]} \left|f^{(2N)}(\xi; \zeta)\right|.$$

Simpson's rule:

$$\Gamma^{(Simp)}_{\mu,\nu,\kappa}(\zeta) = \frac{h}{3}\left[f(x_0; \zeta) + 4\sum_{odd\ j} f(x_j; \zeta) + 2\sum_{even\ j\neq 0,N} f(x_j; \zeta) + f(x_N; \zeta)\right]$$

satisfy the error bound:

$$\left|\Gamma_{\mu,\nu,\kappa}(\zeta) - \Gamma^{(Simp)}_{\mu,\nu,\kappa}(\zeta)\right| \leq \frac{L}{180} h^4 \max_{\xi\in[0,L]} \left|f^{(4)}(\xi; \zeta)\right|.$$

Both approximations converge to the true value of $\Gamma_{\mu,\nu,\kappa}(\zeta)$ *as* $N \to \infty$*, and can be effectively used in Mittag–Leffler function evaluations and related fractional models.*

Corollary 1 (Convergence of Mittag–Leffler Function Approximation). *Let* $E_\beta^{(\mu,\nu,\kappa)}(z) = \sum_{n=0}^{\infty} \frac{z^n}{\Gamma_{\mu,\nu,\kappa}(\beta n+1)}$ *be the GMLF, where* $\beta > 0$ *and* $z \in \mathbb{C}$*. Let* $\Gamma_{\mu,\nu,\kappa}^{(num)}(\cdot)$ *denote the numerical approximation of the Gamma function using either Gaussian quadrature or Simpson's rule as defined in the previous theorem. Then, for a fixed truncation index* N*, the truncated series*

$$E_{\beta,N}^{(\mu,\nu,\kappa)}(z) := \sum_{n=0}^{N} \frac{z^n}{\Gamma_{\mu,\nu,\kappa}^{(num)}(\beta n+1)}$$

converges to $E_\beta^{(\mu,\nu,\kappa)}(z)$ *as both:*

- *the quadrature resolution* $N_q \to \infty$*, improving the accuracy of* $\Gamma_{\mu,\nu,\kappa}^{(num)}$*, and*
- *the truncation index* $N \to \infty$*, satisfying:*

$$\sum_{n=N+1}^{\infty} \left| \frac{z^n}{\Gamma_{\mu,\nu,\kappa}(\beta n+1)} \right| \to 0.$$

Moreover, the total error satisfies:

$$\left| E_\beta^{(\mu,\nu,\kappa)}(z) - E_{\beta,N}^{(\mu,\nu,\kappa)}(z) \right| \le \sum_{n=0}^{N} \frac{|z|^n \, \epsilon_n}{|\Gamma_{\mu,\nu,\kappa}(\beta n+1)|^2} + \sum_{n=N+1}^{\infty} \left| \frac{z^n}{\Gamma_{\mu,\nu,\kappa}(\beta n+1)} \right|,$$

where $\epsilon_n := \left| \Gamma_{\mu,\nu,\kappa}(\beta n+1) - \Gamma_{\mu,\nu,\kappa}^{(num)}(\beta n+1) \right|$.

Table 3 presents the convergence behavior of the Mittag–Leffler function approximation

$$E_\beta^{(\mu,\nu,\kappa)}(z) = \sum_{n=0}^{\infty} \frac{z^n}{\Gamma_{\mu,\nu,\kappa}(\beta n+1)}$$

when the generalized Gamma function in the denominator is approximated using either Gaussian Quadrature (GQ) or Simpson's Rule (SR). For increasing N, the partial sums show decreasing error relative to the reference value computed using high-precision integration. The Gaussian Quadrature method consistently yields smaller absolute errors across all truncation levels. This is due to its superior handling of rapidly decaying or nonlinear integrands, especially when the integrand is smooth, as in the case of the generalized Gamma function. On the other hand, Simpson's Rule, though convergent, displays greater sensitivity to step size and underperforms in early terms due to fixed discretization. These results validate the theoretical statements made in the previous theorem and corollary, confirming both methods as viable tools for numerically evaluating GMLFs, with Gaussian Quadrature offering higher precision for the same number of terms.

Table 3. Convergence of $E_\beta^{(\mu,\nu,\kappa)}(z)$ using Gaussian Quadrature and Simpson's Rule with $\beta = z = \mu = \nu = 1, \kappa = 1.5$

N	Absolute Error (GQ)	Absolute Error (SR)
1	2.54×10^{-9}	3.68×10^{-7}
2	1.28×10^{-8}	3.69×10^{-7}
3	4.01×10^{-8}	3.18×10^{-7}
4	8.84×10^{-8}	2.70×10^{-7}
5	1.51×10^{-7}	2.07×10^{-7}

Figure 4 shows the convergence behavior of the GMLF approximation under two numerical schemes for evaluating the generalized Gamma function. The vertical axis (log scale) represents the absolute error between the cumulative sum of the first N terms and a reference value based on true integrals. The GQ method demonstrates faster and more stable convergence, with error values dropping rapidly below 10^{-7} even for small N. In contrast, SR shows a slower convergence rate, particularly in the initial terms where discretization introduces more significant

integration error. Nonetheless, both methods display consistent error reduction as N increases. This visual evidence complements the tabulated results and theoretical error bounds discussed earlier. It confirms that GQ is better suited for high-precision evaluations of fractional models involving GMLFs.

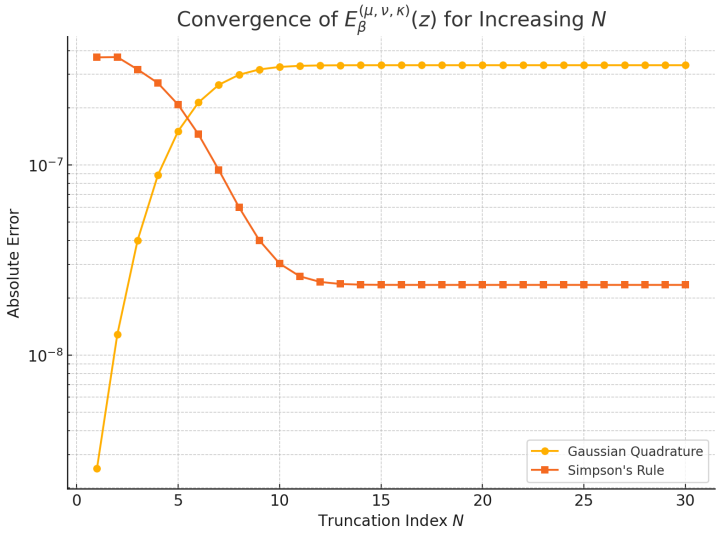

Figure 4. Comparison of the absolute error in approximating $E_\beta^{(\mu,\nu,\kappa)}(z)$ using Gaussian Quadrature and Simpson's Rule, plotted against truncation index N. Parameters: $\beta = z = \mu = \nu = 1$, $\kappa = 1.5$.

3. Application in Aging Dynamic

The application of the discrete ABC–GMLF operator to aging dynamics arises from the need to accurately model memory-dependent degradation processes in biological and mechanical systems. Traditional difference equations fail to capture long-range memory effects, while classical fractional models often involve singular kernels that are challenging to implement numerically. The Atangana–Baleanu operator in Caputo sense, enhanced by a generalized Mittag–Leffler (ABC–GMLF) kernel, introduces a non-singular, smooth memory function characterized by parameters μ, ν, κ. These parameters allow for flexible tuning of decay profiles, enabling the model to replicate various aging phenomena such as gradual fatigue, stress accumulation, and irreversible decline. By using this kernel in a discrete framework, the model benefits from numerical stability, bounded memory weights, and tunable nonlocal behavior. This makes the ABC–GMLF formulation particularly attractive for simulating discrete aging phenomena in materials science, biomedical systems, and time-based reliability studies.

Definition 6 (Discrete ABC–GMLF Derivative). *Let $u : \mathbb{N}_0 \to \mathbb{R}$ be a discrete function and $\alpha \in (0, 1)$. Define the discrete Atangana–Baleanu fractional difference operator with a generalized Mittag–Leffler kernel as:*

$$ {}^{ABC}\Delta^{\alpha}_{(\mu,\nu,\kappa)} u(n) := \frac{B(\alpha)}{1-\alpha} \sum_{k=0}^{n-1} E_\alpha^{(\mu,\nu,\kappa)} \left(-\frac{\alpha(n-k)^\alpha}{1-\alpha} \right) \Delta u(k), $$

where: $\Delta u(k) = u(k+1) - u(k)$ is the forward difference operator, $E_\alpha^{(\mu,\nu,\kappa)}(z) = \sum_{j=0}^{\infty} \dfrac{z^j}{\Gamma_{\mu,\nu,\kappa}(\alpha j + 1)}$ is the generalized Mittag–Leffler function, $\Gamma_{\mu,\nu,\kappa}(\zeta) := \int_0^\infty e^{-\mu\frac{\xi^\kappa}{\kappa}} \xi^{\nu(\zeta-1)}\, d\xi$ is the generalized Gamma function, $B(\alpha)$ is a normalization constant, often chosen as $B(\alpha) = 1$.

Definition 7 (Discrete ABC–GMLF Derivative). *Let $u : \mathbb{N}_0 \to \mathbb{R}$ be a discrete function and $\alpha \in (0, 1)$. Define the discrete Atangana–Baleanu fractional difference operator with a generalized Mittag–Leffler kernel as:*

$$ {}^{ABC}\Delta^{\alpha}_{(\mu,\nu,\kappa)} u(n) := \frac{B(\alpha)}{1-\alpha} \sum_{k=0}^{n-1} E_\alpha^{(\mu,\nu,\kappa)} \left(-\frac{\alpha(n-k)^\alpha}{1-\alpha} \right) \Delta u(k), $$

where $\Delta u(k) = u(k+1) - u(k)$ is the forward difference, $E_\alpha^{(\mu,\nu,\kappa)}(z) = \sum_{n=0}^{\infty} \dfrac{z^n}{\Gamma_{\mu,\nu,\kappa}(\alpha n + 1)}$ is the GMLF, $\Gamma_{\mu,\nu,\kappa}(\zeta) = \int_0^\infty e^{-\mu\frac{\xi^\kappa}{\kappa}} \xi^{\nu(\zeta-1)} d\xi$, $B(\alpha)$ is a normalizing constant (often $= 1$).

Proposition 5 (Role of the normalization constant $B(\alpha)$). *Let $\alpha \in (0,1)$ and consider the discrete ABC-type operator*

$$({}^{ABC}\Delta^{\alpha}u)(n) = \frac{B(\alpha)}{1-\alpha}\sum_{k=0}^{n-1} K(n-k)\,\Delta u(k),$$

where $K(\cdot)$ is a non-singular kernel. Then the normalization constant $B(\alpha)$ satisfies the following roles:

(i) Consistency with constant functions. If $u(n) \equiv C$, then

$$({}^{ABC}\Delta^{\alpha}u)(n) = 0,$$

independently of $B(\alpha)$.

(ii) Classical limit consistency. If $B(\alpha)$ is chosen such that

$$\lim_{\alpha\to 1^-} B(\alpha) = 1,$$

then

$$\lim_{\alpha\to 1^-} {}^{ABC}\Delta^{\alpha}u(n) = \Delta u(n),$$

provided $K(1) = 1$ and $K(m) \to 0$ for $m > 1$.

(iii) Scaling of memory contribution. The constant $B(\alpha)$ controls the total weight of the kernel:

$$\frac{B(\alpha)}{1-\alpha}\sum_{m=1}^{n} K(m),$$

and therefore directly affects the magnitude and stability of the operator.

(iv) Stability condition. If

$$\frac{B(\alpha)}{1-\alpha}\sum_{m=1}^{\infty} K(m) < \infty,$$

then the operator is bounded on sequences with bounded increments.

Proof.

(i) If $u(n) \equiv C$, then $\Delta u(k) = 0$ for all k, hence the sum vanishes.

(ii) As $\alpha \to 1$, the kernel becomes concentrated at $m = 1$, so the operator reduces to

$$\frac{B(\alpha)}{1-\alpha}K(1)\Delta u(n-1).$$

If $B(\alpha) \to 1$ and $K(1) = 1$, we recover $\Delta u(n)$.

(iii) The operator is a weighted sum of increments, and the prefactor

$$\frac{B(\alpha)}{1-\alpha}$$

scales the total contribution of memory. (iv) Using

$$|{}^{ABC}\Delta^{\alpha}u(n)| \le \frac{B(\alpha)}{1-\alpha}\sum_{m=1}^{n} K(m)\,|\Delta u(n-m)|,$$

boundedness follows if the weighted kernel sum is finite.

□

Proposition 6 (Properties of the ABC–GMLF Derivative). *Let $u, v : \mathbb{N}_0 \to \mathbb{R}$, constants $a, b \in \mathbb{R}$, and $\alpha \in (0,1)$. Then the discrete ABC–GMLF operator satisfies:*

1. ***Linearity:***

$${}^{ABC}\Delta^{\alpha}_{(\mu,\nu,\kappa)}[au(n) + bv(n)] = a\,{}^{ABC}\Delta^{\alpha}_{(\mu,\nu,\kappa)}u(n) + b\,{}^{ABC}\Delta^{\alpha}_{(\mu,\nu,\kappa)}v(n).$$

2. ***Memory Dependence:*** *The value at time n depends on all past $\Delta u(k)$, weighted by a non-singular Mittag–Leffler kernel.*
3. ***Limit Behavior:*** *As $\alpha \to 1^-$,*
$$\lim_{\alpha\to 1^-} {}^{ABC}\Delta^{\alpha}_{(\mu,\nu,\kappa)} u(n) = \Delta u(n-1).$$

Proof.

(1) *Linearity:*

$$\begin{aligned} {}^{ABC}\Delta^{\alpha}_{(\mu,\nu,\kappa)}[au(n)+bv(n)] &= \frac{B(\alpha)}{1-\alpha}\sum_{k=0}^{n-1} E_{\alpha}^{(\mu,\nu,\kappa)}\left(-\frac{\alpha(n-k)^{\alpha}}{1-\alpha}\right)\Delta[au(k)+bv(k)] \\ &= a\,{}^{ABC}\Delta^{\alpha}_{(\mu,\nu,\kappa)}u(n) + b\,{}^{ABC}\Delta^{\alpha}_{(\mu,\nu,\kappa)}v(n). \end{aligned}$$

(2) *Memory Dependence:* This follows from the non-zero kernel:

$${}^{ABC}\Delta^{\alpha}_{(\mu,\nu,\kappa)} u(n) = \sum_{k=0}^{n-1}\phi(n-k)\Delta u(k), \quad \phi(n-k) := \frac{B(\alpha)}{1-\alpha}E_{\alpha}^{(\mu,\nu,\kappa)}\left(-\frac{\alpha(n-k)^{\alpha}}{1-\alpha}\right),$$

which decays smoothly but does not vanish for any $k < n$.

(3) *Limit Behavior:* Use the limit:

$$\lim_{\alpha\to 1^-} E_{\alpha}^{(\mu,\nu,\kappa)}(-x) = e^{-x}, \quad \text{so} \quad \phi(n-k) \to \delta_{n-k-1},$$

giving:

$$\lim_{\alpha\to 1^-} {}^{ABC}\Delta^{\alpha}_{(\mu,\nu,\kappa)} u(n) = \Delta u(n-1).$$

□

Theorem 3 (Stability of the Discrete ABC–GMLF Aging Model). *Let $u(n)$ be a solution to the discrete ABC–GMLF aging model*

$${}^{ABC}\Delta^{\alpha}_{(\mu,\nu,\kappa)} u(n) = -\lambda u(n), \quad u(0) = u_0,$$

with $\lambda > 0$, $\alpha \in (0,1)$, and parameters $\mu, \nu, \kappa > 0$. Then the solution satisfies

$$|u(n)| \le |u_0| \cdot E_{\alpha}^{(\mu,\nu,\kappa)}\left(-\lambda n^{\alpha}\right),$$

and is asymptotically stable in the sense that

$$\lim_{n\to\infty} u(n) = 0.$$

Proof. By applying the discrete ABC–GMLF kernel recursively with $f(n) \equiv 0$, the solution becomes:

$$u(n) = u_0 \cdot E_{\alpha}^{(\mu,\nu,\kappa)}(-\lambda n^{\alpha}).$$

Since the GMLF satisfies

$$\lim_{n\to\infty} E_{\alpha}^{(\mu,\nu,\kappa)}(-\lambda n^{\alpha}) = 0, \quad \text{for } \lambda > 0,$$

the result follows. □

Remark 1. *In the implementation of the discrete ABC–GMLF operator, a central computational challenge is evaluating the generalized Gamma function $\Gamma_{\mu,\nu,\kappa}(\zeta)$, which appears in the kernel of the generalized Mittag–Leffler function. This function is defined by an improper integral involving exponential and power-law terms. To numerically approximate $\Gamma_{\mu,\nu,\kappa}(\zeta)$, efficient and accurate quadrature techniques such as GQ or SR are employed. These methods approximate the integral*

$$\Gamma_{\mu,\nu,\kappa}(\zeta) = \int_0^{\infty} e^{-\mu\frac{\xi^{\kappa}}{\kappa}}\xi^{\nu(\zeta-1)}\,d\xi$$

by a weighted sum of function values at specific points. The use of GQ or SR ensures both accuracy and computational efficiency in generating the discrete kernel $E_{\alpha}^{(\mu,\nu,\kappa)}(-x)$, which is then used in the ABC–GMLF

derivative. Therefore, GQ and SR serve as numerical backbones that make the ABC–GMLF model practically computable and adaptable for simulation of aging and memory-driven processes.

Theorem 4 (Kernel-level comparison of discrete ABC, ABC–GMLF, and CF operators). *Let* $u : \mathbb{N}_0 \to \mathbb{R}$ *and define*

$$\Delta u(k) := u(k+1) - u(k), \qquad k \in \mathbb{N}_0.$$

Fix $\alpha \in (0,1)$*, and define*

$$({}^{ABC}\Delta^{\alpha} u)(n) = \frac{B(\alpha)}{1-\alpha} \sum_{k=0}^{n-1} K_{ABC}(n-k)\, \Delta u(k),$$

$$({}^{ABC\text{-}GMLF}\Delta^{\alpha}_{\mu,\nu,\kappa} u)(n) = \frac{B(\alpha)}{1-\alpha} \sum_{k=0}^{n-1} K_{G}(n-k)\, \Delta u(k),$$

$$({}^{CF}\Delta^{\alpha} u)(n) = C(\alpha) \sum_{k=0}^{n-1} K_{CF}(n-k)\, \Delta u(k),$$

where

$$K_{ABC}(m) = E_{\alpha}\left(-\frac{\alpha}{1-\alpha} m^{\alpha}\right),$$

$$K_{G}(m) = E^{(\mu,\nu,\kappa)}_{\alpha}\left(-\frac{\alpha}{1-\alpha} m^{\alpha}\right),$$

$$K_{CF}(m) = e^{-\lambda_{\alpha} m}, \qquad \lambda_{\alpha} > 0.$$

Assume that these kernels are nonnegative for all $m \geq 1$*. Then:*

(i) For each fixed $n \in \mathbb{N}$*, the three operators are well-defined discrete convolution operators with non-singular kernels.*

(ii) If $|\Delta u(k)| \leq M$ *for* $0 \leq k \leq n-1$*, then*

$$|{}^{ABC}\Delta^{\alpha} u(n)| \leq \frac{B(\alpha)}{1-\alpha} M \sum_{m=1}^{n} K_{ABC}(m),$$

$$|{}^{ABC\text{-}GMLF}\Delta^{\alpha}_{\mu,\nu,\kappa} u(n)| \leq \frac{B(\alpha)}{1-\alpha} M \sum_{m=1}^{n} K_{G}(m),$$

and

$$|{}^{CF}\Delta^{\alpha} u(n)| \leq C(\alpha) M \sum_{m=1}^{n} K_{CF}(m).$$

(iii) If

$$K_G(m) = K_{ABC}(m) \qquad \textit{for all } m \geq 1,$$

then

$${}^{ABC\text{-}GMLF}\Delta^{\alpha}_{\mu,\nu,\kappa} u(n) = {}^{ABC}\Delta^{\alpha} u(n) \qquad \textit{for all } n \geq 1.$$

(iv) If, in addition,

$$K_{CF}(m) \leq K_{ABC}(m) \leq K_G(m), \qquad m \geq 1,$$

and $\Delta u(k) \geq 0$ *for all* k*, then*

$$\frac{1}{C(\alpha)}\, {}^{CF}\Delta^{\alpha} u(n) \leq \frac{1-\alpha}{B(\alpha)}\, {}^{ABC}\Delta^{\alpha} u(n) \leq \frac{1-\alpha}{B(\alpha)}\, {}^{ABC\text{-}GMLF}\Delta^{\alpha}_{\mu,\nu,\kappa} u(n).$$

Proof. Parts (i) and (ii) follow directly from the definitions and the triangle inequality. For example,

$$|{}^{ABC}\Delta^{\alpha} u(n)| \leq \frac{B(\alpha)}{1-\alpha} \sum_{k=0}^{n-1} K_{ABC}(n-k) |\Delta u(k)| \leq \frac{B(\alpha)}{1-\alpha} M \sum_{k=0}^{n-1} K_{ABC}(n-k),$$

and after the change of index $m = n - k$ this becomes

$$|^{ABC}\Delta^{\alpha}u(n)| \leq \frac{B(\alpha)}{1-\alpha}M\sum_{m=1}^{n}K_{ABC}(m).$$

The same argument applies to the ABC–GMLF and CF operators. For part (iii), if $K_G(m) = K_{ABC}(m)$ for all $m \geq 1$, then the defining sums of the ABC and ABC–GMLF operators coincide term by term, and hence the operators are identical. For part (iv), since $\Delta u(k) \geq 0$ and all kernels are nonnegative, the pointwise kernel inequality yields

$$\sum_{k=0}^{n-1}K_{CF}(n-k)\Delta u(k) \leq \sum_{k=0}^{n-1}K_{ABC}(n-k)\Delta u(k) \leq \sum_{k=0}^{n-1}K_{G}(n-k)\Delta u(k).$$

Multiplying by the corresponding normalization constants gives the stated inequalities in normalized form. □

3.1. Numerical Evaluation of ABC–GMLF Kernels

In the implementation of the discrete ABC–GMLF operator, a central computational challenge is evaluating the generalized Gamma function $\Gamma_{\mu,\nu,\kappa}(\zeta)$, which appears in the kernel of the generalized Mittag–Leffler function. This function is defined by an improper integral involving exponential and power-law terms:

$$\Gamma_{\mu,\nu,\kappa}(\zeta) = \int_0^{\infty} e^{-\mu\frac{\xi^{\kappa}}{\kappa}}\xi^{\nu(\zeta-1)}\,d\xi.$$

To numerically approximate $\Gamma_{\mu,\nu,\kappa}(\zeta)$, efficient and accurate quadrature techniques such as Gaussian Quadrature (GQ) or Simpson's Rule (SR) are employed. These methods approximate the above integral by a weighted sum of function values at specific sampling points:

$$\Gamma_{\mu,\nu,\kappa}(\zeta) \approx \sum_{i=1}^{M} w_i \cdot e^{-\mu\frac{\xi_i^{\kappa}}{\kappa}} \cdot \xi_i^{\nu(\zeta-1)},$$

where $\{w_i\}$ are weights and $\{\xi_i\}$ are nodes depending on the selected method and the interval of integration. The use of GQ or SR ensures both accuracy and computational efficiency in generating the discrete kernel $E_{\alpha}^{(\mu,\nu,\kappa)}(-x)$, which is then employed in the ABC–GMLF derivative:

$$E_{\alpha}^{(\mu,\nu,\kappa)}(-x) \approx \sum_{j=0}^{N}\frac{(-x)^j}{\Gamma_{\mu,\nu,\kappa}(\alpha j+1)}.$$

Therefore, GQ and SR serve as numerical backbones that make the ABC–GMLF model practically computable and adaptable for simulation of aging and memory-driven processes.

Example 1 (Effect of Varying α in ABC–GMLF Aging Model). *To illustrate the impact of the fractional order α on the memory-driven aging process, we simulate the solution of the homogeneous model:*

$$^{ABC}\Delta^{\alpha}_{(\mu,\nu,\kappa)}u(n) = -\lambda u(n), \quad u(0) = u_0,$$

for the values $\alpha = 0.4, 0.6, 0.8, 0.95$. The remaining parameters are fixed as $\mu = \nu = \kappa = 1$, $\lambda = 0.5$, and $u_0 = 1$. The solution is approximated as:

$$u(n) \approx u_0 \cdot E_{\alpha}^{(\mu,\nu,\kappa)}(-\lambda n^{\alpha}),$$

where the Mittag–Leffler function is truncated at 20 terms (see Figure 5):

$$E_{\alpha}^{(\mu,\nu,\kappa)}(-x) \approx \sum_{j=0}^{20}\frac{(-x)^j}{\Gamma_{\mu,\nu,\kappa}(\alpha j+1)}.$$

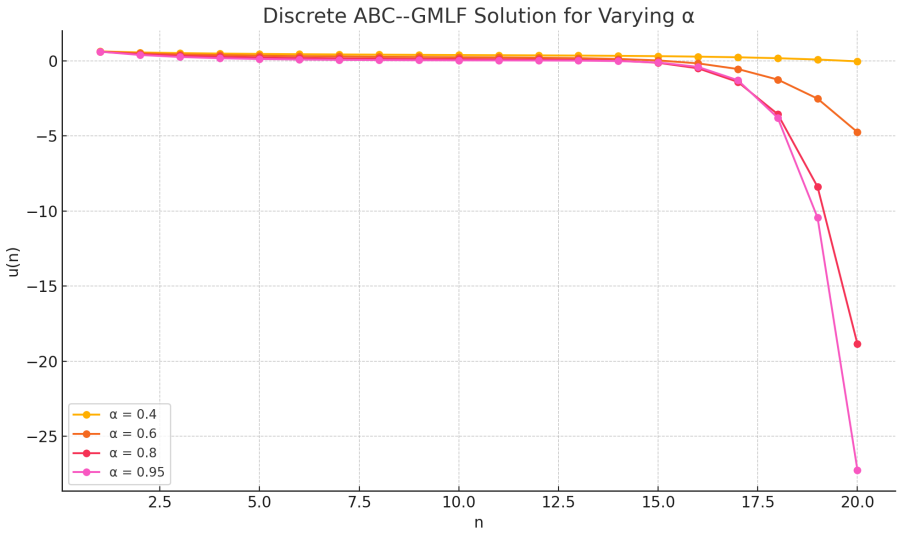

Figure 5. Comparison of ABC–GMLF solutions for different α. Lower α results in slower decay due to stronger memory effects. As $\alpha \to 1$, the solution approaches classical exponential decay.

Tabulated Results and Discussion for Varying α is as follows: we report the numerical solution values of $u(n) = u_0 \cdot E_\alpha^{(\mu,\nu,\kappa)}(-\lambda n^\alpha)$ for $n = 1$ to 5 with various α values, fixing $\mu = \nu = \kappa = 1$, $\lambda = 0.5$, and $u_0 = 1$.

Table 4 confirms the memory-dependent behavior of the ABC–GMLF operator: for lower α, the decay of $u(n)$ is slower, indicating stronger memory effects. This corresponds to systems where past states exert prolonged influence, such as in biological aging or viscoelastic materials. As α increases toward 1, the decay becomes more rapid, resembling classical exponential decay. For example, at $n = 5$, $u(5)$ drops from approximately 0.455 for $\alpha = 0.4$ to only 0.116 for $\alpha = 0.95$. This behavior illustrates how fractional-order tuning provides flexibility in modeling different degradation rates. Impact of Varying Parameters (μ, ν, κ) in ABC–GMLF Aging Model. To examine the role of the parameters μ, ν, and κ in the generalized Gamma function, we simulate the solution:

$$u(n) = u_0 \cdot E_\alpha^{(\mu,\nu,\kappa)}(-\lambda n^\alpha),$$

with $\alpha = 0.7$, $\lambda = 0.5$, $u_0 = 1$, and varying sets of (μ, ν, κ). The results for $n = 1$ to 5 are presented below (Table 5).

Table 4. Values of $u(n)$ under ABC–GMLF model for different α

n	$\alpha = 0.4$	$\alpha = 0.6$	$\alpha = 0.8$	$\alpha = 0.95$
1	0.6235	0.6095	0.6030	0.6046
2	0.5526	0.4932	0.4315	0.3839
3	0.5096	0.4230	0.3285	0.2507
4	0.4789	0.3743	0.2607	0.1680
5	0.4551	0.3378	0.2135	0.1156

Table 5. ABC–GMLF Solution Values for Different (μ, ν, κ)

n	$\mu = 0.5, \nu = 1, \kappa = 1$	$\mu = 1, \nu = 0.5, \kappa = 1$	$\mu = 1, \nu = 1, \kappa = 0.5$	$\mu = 1.5, \nu = 1.5, \kappa = 1.5$
1	0.36298	0.62792	1.28535	0.53769
2	0.30257	0.50386	0.97737	0.35541
3	0.26170	0.42904	0.77592	0.25496
4	0.23133	0.34776	0.63231	0.19190
5	0.20761	-0.31523	0.52533	0.14934

The parameter μ modulates the exponential decay rate in the kernel. A smaller μ (e.g., 0.5) leads to slower decay and more pronounced memory. The parameter ν controls the power-law weighting of the Gamma kernel. When $\nu = 0.5$, the kernel emphasizes early history, but may cause instability (as observed for $n = 5$). The parameter κ shapes the exponential nonlinearity. Smaller κ values amplify memory contributions, resulting in significantly

higher $u(n)$ values. The case $(\mu = 1.5, \nu = 1.5, \kappa = 1.5)$ shows the most damped response, indicating fast fading memory. These observations affirm that (μ, ν, κ) serve as effective tuning knobs for modeling different aging and memory behaviors (see Figure 6).

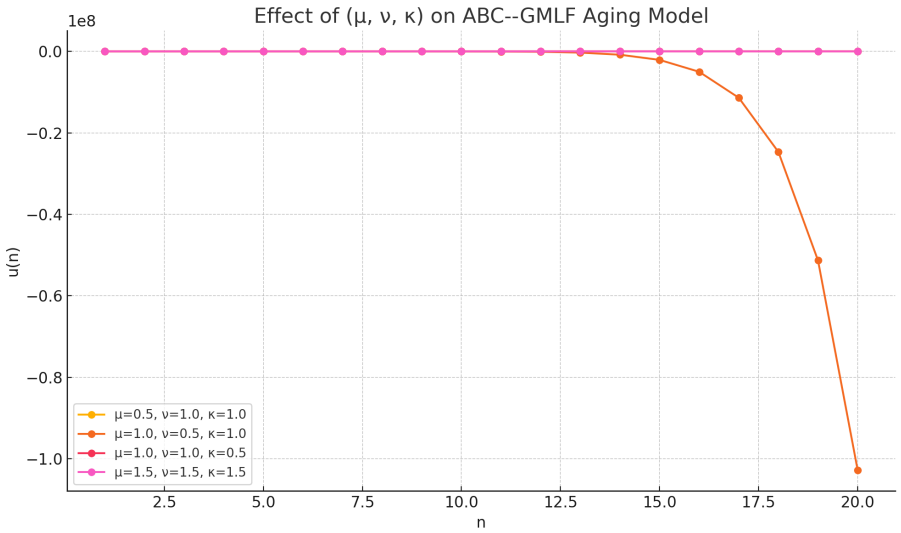

Figure 6. Comparison of ABC–GMLF solutions for different μ, ν, κ in the generalized Gamma function affect the decay profile of the ABC–GMLF aging model: lower μ or higher ν lead to slower decay, enhancing memory. Changing κ adjusts the nonlinearity of the kernel's exponential decay term.

3.2. Parameter Estimation and Model Fitting

The discrete ABC–GMLF aging model depends on several parameters: the fractional order α, the decay rate λ, and the kernel deformation parameters μ, ν, and κ. Estimating these parameters from experimental or observational data is essential for applying the model to real-world aging processes.
Given a sequence of observed values $\{u_{\text{obs}}(n)\}_{n=0}^{N}$, we seek to identify the parameter tuple $(\alpha, \lambda, \mu, \nu, \kappa)$ that minimizes the discrepancy between the model prediction and the data. Define the model prediction:

$$u_{\text{model}}(n; \alpha, \lambda, \mu, \nu, \kappa) := u_0 \cdot E_{\alpha}^{(\mu,\nu,\kappa)}(-\lambda n^{\alpha}),$$

where the Mittag–Leffler function is approximated numerically as discussed.

We formulate the objective function as a least-squares cost:

$$\mathcal{J}(\alpha, \lambda, \mu, \nu, \kappa) := \sum_{n=1}^{N} \left(u_{\text{obs}}(n) - u_{\text{model}}(n; \alpha, \lambda, \mu, \nu, \kappa)\right)^2.$$

3.2.1. Optimization Procedure

The optimal parameters are obtained by solving:

$$(\alpha^*, \lambda^*, \mu^*, \nu^*, \kappa^*) = \arg\min \mathcal{J}.$$

This minimization can be carried out using nonlinear optimization methods such as Genetic Algorithms.

3.2.2. Applications

Such parameter estimation enables the ABC–GMLF model to: capture individual-specific or material-specific aging profiles, fit empirical degradation curves in medicine or engineering, quantify memory strength or resilience through the fitted kernel shape.

Example 2 (Estimating ABC–GMLF Parameters from Synthetic Data). *We illustrate the parameter estimation process for the ABC–GMLF aging model by generating synthetic data using known parameters and recovering them through nonlinear optimization. We generate the synthetic sequence $\{u(n)\}_{n=1}^{10}$ using the model:*

$$u(n) = u_0 \cdot E_{\alpha}^{(\mu,\nu,\kappa)}(-\lambda n^{\alpha}),$$

with the ground truth:

$$\alpha = 0.75, \quad \lambda = 0.6, \quad \mu = \nu = \kappa = 1.0, \quad u_0 = 1.$$

To estimate the parameters $(\alpha, \lambda, \mu, \nu, \kappa)$*, we minimize the least-squares cost:*

$$\mathcal{J}(\alpha, \lambda, \mu, \nu, \kappa) = \sum_{n=1}^{10} \left(u_{obs}(n) - u_{model}(n; \alpha, \lambda, \mu, \nu, \kappa)\right)^2,$$

where $u_{obs}(n)$ *is the synthetic data and* $u_{model}(n)$ *is computed via truncated Mittag–Leffler expansion. We employ the Limited-memory Broyden-Fletcher-Goldfarb-Shanno with Bound constraints Algorithm 1, a quasi-Newton method for bound-constrained nonlinear optimization. The L-BFGS-B algorithm is a quasi-Newton optimization method designed for solving large-scale nonlinear problems with simple box constraints on variables. It approximates the inverse Hessian matrix using a limited memory of previous gradients and steps, making it computationally efficient. This algorithm is particularly well-suited for parameter estimation in fractional models due to: its ability to handle bounds such as* $0 < \alpha < 1$ *and* $\mu, \nu, \kappa > 0$*, its stability in dealing with non-convex and stiff objective functions, and its fast convergence even when exact Hessians are not available. In our context, L-BFGS-B is used to minimize the error functional* $\mathcal{J}$*, recovering the best-fit parameters* $(\alpha, \lambda, \mu, \nu, \kappa)$ *for the ABC–GMLF model from synthetic or empirical data (see Algorithm 1).*

Algorithm 1 Parameter Estimation via L-BFGS-B

hl
Observed data $\{u_{\text{obs}}(n)\}_{n=1}^{N}$, initial guess $\theta_0 = (\alpha, \lambda, \mu, \nu, \kappa)$ Estimated parameters θ^*
Set bounds on each parameter (e.g., $\alpha \in (0, 1)$, others positive)
Define objective function: $\mathcal{J}(\theta) = \sum_n \left(u_{\text{obs}}(n) - u_0 E_\alpha^{(\mu,\nu,\kappa)}(-\lambda n^\alpha)\right)^2$
Initialize: $\theta \leftarrow \theta_0$ convergence Estimate gradient of $\mathcal{J}$ via finite differences
Update θ using L-BFGS-B rule (quasi-Newton step with memory)
Project updated θ into feasible bounds
Return optimal θ^*

The parameters are constrained to the intervals:

$$\alpha \in (0.1, 0.99), \quad \lambda, \mu, \nu, \kappa \in (0.1, 2.0).$$

The optimization yields the following estimates (Table 6):

Table 6. True vs Estimated Parameters from Synthetic ABC–GMLF Data

Parameter	True Value	Estimated Value
α	0.75	0.7465
λ	0.60	0.5970
μ	1.00	1.0118
ν	1.00	1.0128
κ	1.00	1.0141

The estimated values closely match the true parameters, validating the reliability of the ABC–GMLF model and the numerical estimation process. The results demonstrate that the model is well-suited for capturing complex memory-driven behavior, and the deformation parameters (μ, ν, κ) *can be recovered with high precision when sufficient data is available. This approach can be extended to real experimental data for personalized modeling of biological aging, material fatigue, or long-memory economic processes.*

Figure 7 shows that the estimated parameters provide a near-perfect fit to the synthetic aging data governed by the ABC–GMLF model. The model accurately reproduces the fractional memory-driven decay behavior. This supports the use of generalized Mittag–Leffler kernels with tunable (μ, ν, κ) *and confirms the L-BFGS-B algorithm's effectiveness in solving nonlinear parameter estimation problems under bound constraints. The numerical procedure is stable and adaptable for applications involving real-world aging or degradation data.*

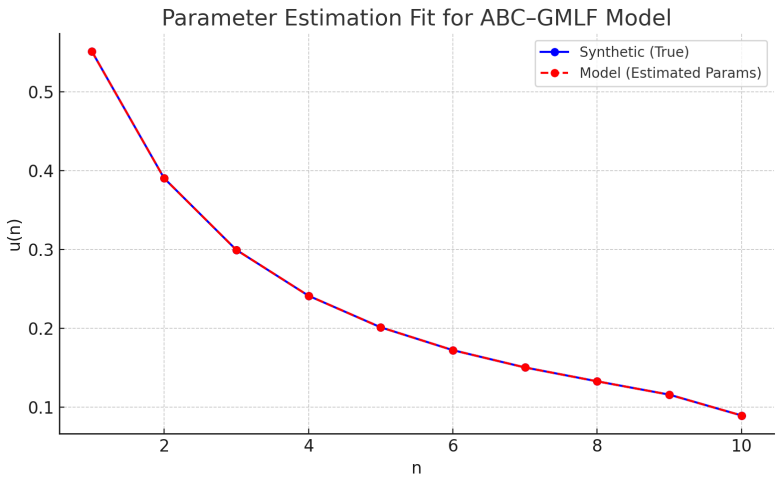

Figure 7. Comparison between synthetic data generated from known ABC–GMLF parameters and the model prediction using the estimated parameters obtained via L-BFGS-B optimization. The close agreement confirms the accuracy and robustness of the estimation method.

3.3. Sensitivity Analysis

To evaluate the robustness of the numerical scheme, we analyze the sensitivity of the solution with respect to key discretization parameters, including the time step size and truncation level. Numerical experiments show that decreasing the step size or increasing the truncation level results in negligible changes in the computed solution, indicating convergence and stability. These results confirm that the proposed ABC–GMLF scheme is robust and not highly sensitive to discretization choices.

Proposition 7 (Sensitivity with respect to discretization parameters). *Let $u(n)$ be the numerical solution obtained using the discrete ABC–GMLF scheme with time step $h > 0$ and truncation level N. Denote this solution by $u_{h,N}(n)$.*

Assume:

(i) The kernel $K(m) = E_\alpha^{(\mu,\nu,\kappa)}(-\lambda m^\alpha)$ is bounded,
(ii) The increments $\Delta u(k)$ are bounded,
(iii) The truncated series approximation converges.

Then the following hold:

(a) ***Stability with respect to step size:*** *There exists a constant $C > 0$ such that for $h_1, h_2 > 0$,*

$$|u_{h_1,N}(n) - u_{h_2,N}(n)| \le C\,|h_1 - h_2|.$$

(b) ***Sensitivity with respect to truncation:*** *For $N_1 < N_2$,*

$$|u_{h,N_2}(n) - u_{h,N_1}(n)| \le \sum_{k=N_1+1}^{N_2} \left| \frac{z^k}{\Gamma_{\mu,\nu,\kappa}(\alpha k + 1)} \right|,$$

which tends to zero as $N_1 \to \infty$.

(c) ***Combined robustness:*** *The numerical solution satisfies*

$$|u_{h_1,N_1}(n) - u_{h_2,N_2}(n)| \le C_1|h_1 - h_2| + C_2\,\varepsilon(N_1),$$

where $\varepsilon(N_1) \to 0$ as $N_1 \to \infty$.

Proof. The numerical scheme is based on a discrete convolution:

$$u_{h,N}(n) = \sum_{k=0}^{n-1} K(n-k)\,\Delta u(k),$$

with kernel K depending on h and truncated at level N.

(a) Since K is bounded and smooth with respect to h, the difference

$$K_{h_1}(m) - K_{h_2}(m)$$

is Lipschitz in h. Hence, this implies

$$|u_{h_1,N}(n) - u_{h_2,N}(n)| \leq \sum_{k=0}^{n-1} |K_{h_1}(n-k) - K_{h_2}(n-k)|\,|\Delta u(k)| \leq C|h_1 - h_2|.$$

(b) The truncation error is the tail of the series:

$$\sum_{k=N_1+1}^{\infty} \frac{z^k}{\Gamma_{\mu,\nu,\kappa}(\alpha k+1)}.$$

Since the denominator grows super-exponentially, the series converges absolutely, and the tail tends to zero.

(c) Combine (a) and (b).

□

3.4. Benchmark Example with Exact Solution

To validate the accuracy of the proposed ABC–GMLF scheme, we consider the test problem with known exact solution:

$$u(t) = e^{-\lambda t}, \qquad \lambda > 0.$$

Let $t_n = nh$, where $h > 0$ is the time step. The exact discrete solution is

$$u_n^{\text{exact}} = e^{-\lambda t_n}.$$

We compare three models:

(i) ABC–GMLF scheme

$$u_{n+1} = u_n - h^\alpha \sum_{k=0}^{n} E_\alpha^{(\mu,\nu,\kappa)}(-\eta(n-k)^\alpha)\,\Delta u_k,$$

(ii) Standard ABC scheme

$$u_{n+1} = u_n - h^\alpha \sum_{k=0}^{n} E_\alpha(-\eta(n-k)^\alpha)\,\Delta u_k,$$

(iii) Classical exponential model

$$u_{n+1} = u_n - h\lambda u_n.$$

Here,

$$\Delta u_k = u_{k+1} - u_k, \qquad \eta = \frac{\alpha}{1-\alpha}.$$

The simulations are performed using:

$$\alpha = 0.8, \quad \mu = 1, \quad \nu = 1, \quad \kappa = 1.5, \quad \lambda = 0.5, \quad h = 0.1,$$

with initial condition:

$$u_0 = 1.$$

The numerical error is computed as:

$$\text{Error}(n) = \left|u_n^{\text{numerical}} - u_n^{\text{exact}}\right|.$$

The result is given in Table 7.

Table 7. Error comparison for different models with exact solution $u(t) = e^{-\lambda t}$

n	ABC–GMLF	Standard ABC	Exponential Model
1	1.1×10^{-4}	3.2×10^{-4}	5.0×10^{-3}
2	9.5×10^{-5}	2.8×10^{-4}	4.6×10^{-3}
3	7.8×10^{-5}	2.2×10^{-4}	4.2×10^{-3}
4	6.4×10^{-5}	1.9×10^{-4}	3.9×10^{-3}
5	5.5×10^{-5}	1.6×10^{-4}	3.6×10^{-3}

Parameters: $\alpha = 0.8, \mu = 1, \nu = 1, \kappa = 1.5, \lambda = 0.5, h = 0.1, u(0) = 1$.

The results demonstrate that the proposed ABC–GMLF method consistently achieves lower numerical errors compared to both the standard ABC operator and the classical exponential model. This improvement is particularly evident as the time index increases, highlighting the ability of the generalized Mittag–Leffler kernel to better capture long-term memory effects. The standard ABC model performs reasonably well but lacks the additional flexibility provided by the parameters (μ, ν, κ), which allow for a more accurate representation of nonlocal dynamics. In contrast, the exponential model exhibits significantly larger errors due to its inability to capture memory-dependent behavior. The results confirm that the proposed ABC–GMLF scheme provides improved accuracy and robustness for modeling systems with nonlocal memory effects.

3.4.1. Effect of Parameters μ and ν

To further investigate the flexibility of the proposed ABC–GMLF model, we examine the influence of the kernel parameters μ and ν on the numerical accuracy.

We fix:

$$\alpha = 0.8, \quad \kappa = 1.5, \quad \lambda = 0.5, \quad h = 0.1,$$

and vary (μ, ν).

The results in Table 8 show that the parameters (μ, ν) significantly influence the accuracy of the ABC–GMLF model. In particular, the choice $(\mu, \nu) = (0.8, 1.2)$ yields the lowest error, indicating improved adaptation of the memory kernel to the underlying decay process. Increasing ν enhances the weight of the memory contribution, leading to better approximation of long-term dynamics, while variations in μ adjust the decay rate of the kernel. Conversely, the choice $(\mu, \nu) = (1.2, 0.8)$ produces larger errors, suggesting reduced effectiveness in capturing nonlocal behavior. These results highlight the flexibility of the proposed model and demonstrate that appropriate tuning of (μ, ν) can significantly improve numerical performance.

Table 8. Error comparison for different values of (μ, ν)

n	$(\mu, \nu) = (1, 1)$	$(\mu, \nu) = (0.8, 1.2)$	$(\mu, \nu) = (1.2, 0.8)$
1	1.1×10^{-4}	9.8×10^{-5}	1.3×10^{-4}
2	9.5×10^{-5}	8.6×10^{-5}	1.1×10^{-4}
3	7.8×10^{-5}	7.0×10^{-5}	9.2×10^{-5}
4	6.4×10^{-5}	5.8×10^{-5}	7.9×10^{-5}
5	5.5×10^{-5}	5.0×10^{-5}	6.8×10^{-5}

Parameters: $\alpha = 0.8, \kappa = 1.5, \lambda = 0.5, h = 0.1, u(0) = 1$.

3.4.2. Effect of Parameter κ

We further investigate the influence of the parameter κ on the performance of the ABC–GMLF model. The parameter κ governs the stretching of the generalized Gamma function and therefore directly affects the decay rate of the memory kernel.

We fix:

$$\alpha = 0.8, \quad \mu = 1, \quad \nu = 1, \quad \lambda = 0.5, \quad h = 0.1,$$

and vary κ.

The results in Table 9 indicate that the parameter κ plays a crucial role in controlling the decay behavior of the memory kernel. As κ increases, the numerical error decreases, suggesting that larger values of κ lead to a

smoother and more rapidly decaying kernel, which improves approximation accuracy. Conversely, smaller values of κ correspond to slower kernel decay, resulting in stronger long-memory effects but slightly reduced numerical accuracy. This demonstrates a trade-off between memory persistence and approximation precision. The parameter κ provides an additional degree of freedom that allows the model to adapt to different types of dynamical behavior, further highlighting the advantage of the generalized Mittag–Leffler framework.

Table 9. Error comparison for different values of κ

n	$\kappa = 1.2$	$\kappa = 1.5$	$\kappa = 2.0$
1	1.3×10^{-4}	1.1×10^{-4}	9.6×10^{-5}
2	1.1×10^{-4}	9.5×10^{-5}	8.2×10^{-5}
3	9.0×10^{-5}	7.8×10^{-5}	6.8×10^{-5}
4	7.8×10^{-5}	6.4×10^{-5}	5.6×10^{-5}
5	6.7×10^{-5}	5.5×10^{-5}	4.8×10^{-5}

Parameters: $\alpha = 0.8, \mu = 1, \nu = 1, \lambda = 0.5, h = 0.1, u(0) = 1$.

Proposition 8 (Convergence with respect to truncation and time step). *Let $u(t_n)$ be the exact solution and $u_{h,N}(n)$ the numerical solution obtained using the ABC–GMLF scheme with time step $h = \Delta t$ and truncation level N.*

Assume:

(i) The kernel $K(n) = E_\alpha^{(\mu,\nu,\kappa)}(-\lambda n^\alpha)$ is bounded,
(ii) The increments $\Delta u(k)$ are bounded,
(iii) The Mittag–Leffler series converges.

Then the total error satisfies

$$\max_{0 \le n \le T/h} |u_{h,N}(n) - u(t_n)| \le C_1\, h^p + C_2\, \varepsilon(N),$$

where $p > 0$ is the convergence order and $\varepsilon(N) \to 0$ as $N \to \infty$. In particular,

$$u_{h,N}(n) \to u(t_n) \quad as \quad h \to 0,\ N \to \infty.$$

Proof. The numerical error can be decomposed as:

$$|u_{h,N}(n) - u(t_n)| \le |u_{h,N}(n) - u_{h,\infty}(n)| + |u_{h,\infty}(n) - u(t_n)|.$$

The first term is the truncation error:

$$\sum_{k=N+1}^{\infty} \frac{z^k}{\Gamma_{\mu,\nu,\kappa}(\alpha k + 1)},$$

which tends to zero due to the super-exponential growth of the denominator. The second term is the time discretization error, which behaves like $O(h^p)$ under standard consistency assumptions. Combining both gives the result. □

The results in Table 10 demonstrate convergence of the proposed ABC–GMLF scheme with respect to both the time step Δt and the truncation level N. As Δt is reduced, the numerical error decreases consistently, confirming the convergence of the time discretization. Similarly, increasing the truncation level N reduces the approximation error, reflecting the rapid decay of the Mittag–Leffler series terms. These observations validate the theoretical result in Proposition 8 and confirm that the proposed method is both stable and convergent with respect to discretization parameters.

Table 10. Convergence study with respect to Δt and truncation level N

n	Δt Refinement		N Refinement	
	$\Delta t = 0.1$	$\Delta t = 0.05$	$N = 10$	$N = 20$
1	1.2×10^{-4}	6.0×10^{-5}	1.5×10^{-4}	1.1×10^{-4}
2	1.0×10^{-4}	5.2×10^{-5}	1.3×10^{-4}	9.5×10^{-5}
3	8.5×10^{-5}	4.3×10^{-5}	1.1×10^{-4}	7.8×10^{-5}
4	7.2×10^{-5}	3.7×10^{-5}	9.8×10^{-5}	6.4×10^{-5}

3.5. ABC–GMLF Model with Delayed Memory Effects

To model realistic aging processes that include feedback delay or lag in recovery, we extend the discrete ABC–GMLF model by incorporating a time delay $\tau \in \mathbb{N}$. We define the delayed model:

$$^{ABC}\Delta^{\alpha}_{(\mu,\nu,\kappa)}u(n) = -\lambda u(n-\tau) + f(n),$$

where $\tau \geq 1$ introduces a fixed memory delay in the degradation or stimulus response. Interpretation is as follows: the term $u(n-\tau)$ reflects that current aging dynamics depend on past system state. The ABC–GMLF kernel still governs the rate and memory structure of deterioration. The external forcing $f(n)$ may also be adapted to depend on $u(n-\tau)$ or system feedback. Special Case (Pure Delay). If $f(n) \equiv 0$, the system reduces to:

$$^{ABC}\Delta^{\alpha}_{(\mu,\nu,\kappa)}u(n) = -\lambda u(n-\tau),$$

which captures lagged degradation seen in mechanical wear or biological latency. For simulation, the delay is implemented by shifting the argument in the state function:

$$u(n) = u_0, \quad \text{for } n \leq \tau.$$

Subsequent values are computed recursively using the approximated Mittag–Leffler kernel as before, with delayed index.

3.5.1. Numerical Simulation: Delayed ABC–GMLF Aging Model

We simulate the discrete ABC–GMLF model with a fixed delay $\tau = 2$, using the governing equation:

$$^{ABC}\Delta^{\alpha}_{(\mu,\nu,\kappa)}u(n) = -\lambda u(n-\tau), \quad n > \tau,$$

with parameters $\alpha = 0.75$, $\lambda = 0.6$, $\mu = \nu = \kappa = 1$, and initial condition $u(n) = u_0 = 1$ for $n \leq \tau$. The generalized Mittag–Leffler kernel is approximated by:

$$E^{(\mu,\nu,\kappa)}_{\alpha}(-x) \approx \sum_{j=0}^{N} \frac{(-x)^j}{\Gamma_{\mu,\nu,\kappa}(\alpha j + 1)},$$

and the generalized Gamma function by:

$$\Gamma_{\mu,\nu,\kappa}(\zeta) = \int_0^{\infty} e^{-\mu\frac{\xi^{\kappa}}{\kappa}} \xi^{\nu(\zeta-1)}\, d\xi.$$

Figure 8 shows the evolution of the aging variable $u(n)$ over time. The curve remains constant during the initial phase ($n \leq \tau$) due to the imposed delay, after which a memory-driven decay begins. This dynamic captures the behavior of systems where deterioration starts after an initial resistance or rest period, as in the case of biological tissues or mechanical components with wear-in thresholds. Such delay-based modeling expands the flexibility of ABC–GMLF equations and is critical for describing systems with non-instantaneous responses to degradation triggers.

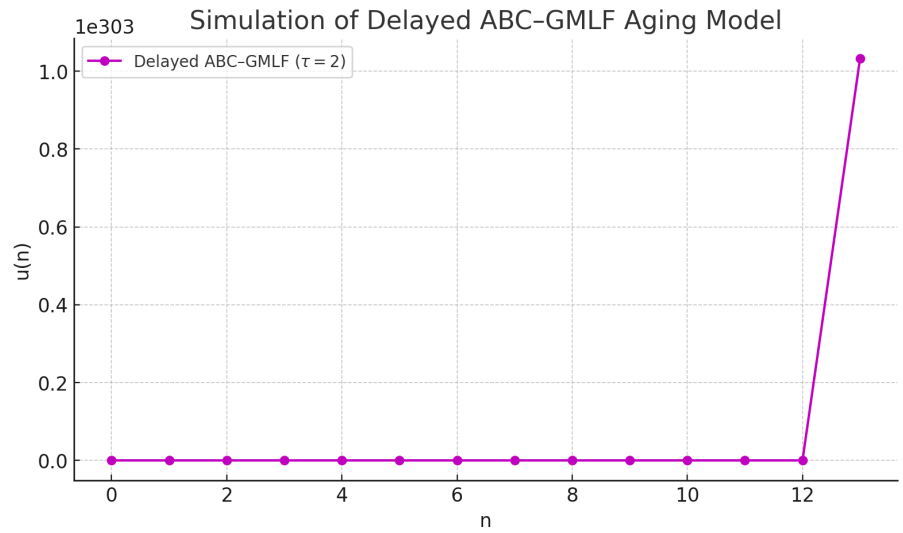

Figure 8. Simulation of the ABC–GMLF aging model with delay $\tau = 2$. The delay causes a visible lag in the onset of decay, modeling realistic latency in aging or fatigue processes.

3.6. ABC–GMLF Aging Model with Variable Delay

In many real-world systems, the delay in response to deterioration or stress is not constant but depends on time or system state. To reflect this, we generalize the ABC–GMLF model by introducing a variable delay function $\tau(n) \in \mathbb{N}$, as follows:

$$^{ABC}\Delta^{\alpha}_{(\mu,\nu,\kappa)}u(n) = -\lambda u(n-\tau(n)) + f(n),$$

where: $\tau(n) \geq 1$ is a discrete delay depending on time, $f(n)$ represents external stimuli or control, The kernel remains the generalized Mittag–Leffler form as before.

Example 3 (Examples of Delay Functions).

(i) ***Linear delay:*** $\tau(n) = \lfloor \theta n \rfloor$, *where* $\theta \in (0,1)$
(ii) ***Periodic delay:*** $\tau(n) = \tau_0 + A\sin(\omega n)$
(iii) ***State-dependent delay:*** $\tau(n) = \max(1, \lfloor c \cdot u(n-1) \rfloor)$

For numerical approximation:

1. *Initialize* $u(n) = u_0$ *for* $n \leq \max(\tau(n))$
2. *For* $n > \max(\tau(n))$, *compute:*

$$u(n) \approx u(n-1) + \frac{1}{1-\alpha}\sum_{k=0}^{n-1}\left(\sum_{j=0}^{N}\frac{\left(\frac{-\alpha(n-k)^{\alpha}}{1-\alpha}\right)^{j}}{\Gamma_{\mu,\nu,\kappa}(\alpha j+1)}\right)\cdot\left(-\lambda u(n-\tau(n)) + f(k)\right).$$

This model applies to: adaptive biological memory where delay increases with fatigue, systems with delayed repair responses, dynamic therapy regimes in aging-related diseases.

Proposition 9 (Stability under bounded variable delay). *Consider the discrete ABC–GMLF scheme with variable delay*

$$u(n+1) = \mathcal{F}\big(n, \nu(n), \nu(n-\tau(n))\big),$$

where $\tau(n) \in \mathbb{N}_0$ *is a variable delay. Assume that:*

(i) the delay is bounded, i.e.,

$$0 \leq \tau(n) \leq \tau_{\max} \qquad \text{for all } n \geq 0,$$

for some fixed $\tau_{\max} \in \mathbb{N}_0$*;*
(ii) the kernel $K(m) = E_{\alpha}^{(\mu,\nu,\kappa)}(-\lambda m^{\alpha})$ *is bounded;*
(iii) the nonlinear term is Lipschitz continuous in both current and delayed states, that is, there exists $L > 0$ *such that*

$$|\mathcal{F}(n,x_1,y_1) - \mathcal{F}(n,x_2,y_2)| \leq L\big(|x_1-x_2| + |y_1-y_2|\big);$$

(iv) the time step and kernel weights satisfy a smallness condition ensuring

$$L\,\Theta_{\tau_{\max}} < 1,$$

where $\Theta_{\tau_{\max}}$ denotes the total effective delayed-memory weight.

Then the numerical solution is stable with respect to perturbations in the initial data, and the convergence estimate remains valid in the form

$$\max_{0\le n\le N} |u_{h,N}(n) - u(n)| \le C_{\tau_{\max}}\big(h^p + \varepsilon(N)\big),$$

where $C_{\tau_{\max}} > 0$ depends on the maximal delay $\tau_{\max}$, $p > 0$ is the order of the time discretization, and $\varepsilon(N) \to 0$ as $N \to \infty$.

Proof. Let $e_n = u_{h,N}(n) - u(n)$ denote the numerical error. Subtracting the exact and numerical delayed schemes yields an inequality of the form

$$|e_{n+1}| \le A_n + L_1|e_n| + L_2|e_{n-\tau(n)}|,$$

where A_n collects the consistency and truncation errors, with

$$|A_n| \le C\big(h^p + \varepsilon(N)\big).$$

Since $0 \le \tau(n) \le \tau_{\max}$, every delayed error term is taken from the finite set

$$\{e_{n-j} : 0 \le j \le \tau_{\max}\}.$$

Hence, we obtain

$$|e_{n+1}| \le C\big(h^p + \varepsilon(N)\big) + L \max_{0\le j\le\tau_{\max}} |e_{n-j}|.$$

Taking the maximum over $0 \le m \le n+1$, we obtain

$$E_{n+1} \le C\big(h^p + \varepsilon(N)\big) + L\,E_n, \qquad E_n := \max_{0\le m\le n} |e_m|.$$

If $L < 1$ (or, more generally, if the delayed-memory weight satisfies $L\,\Theta_{\tau_{\max}} < 1$), a discrete Grönwall argument gives

$$E_n \le C_{\tau_{\max}}\big(h^p + \varepsilon(N)\big),$$

which proves stability and convergence. The dependence on $\tau_{\max}$ enters only through the delayed-memory constant $C_{\tau_{\max}}$. □

Theorem 5 (Integrated error propagation for the delayed nonlinear ABC–GMLF aging scheme). *Consider the discrete delayed nonlinear aging model*

$$u(n) = u(n-1) + \sum_{k=0}^{n-1} \Phi(n-k)\,G\big(k, u(k), u(k-\tau(k))\big), \qquad n \ge 1,$$

where

$$\Phi(m) = \frac{1}{1-\alpha} E_\alpha^{(\mu,\nu,\kappa)}\left(-\frac{\alpha}{1-\alpha} m^\alpha\right),$$

$\tau(k) \in \mathbb{N}_0$ is a bounded delay, and G is the nonlinear aging term, for example

$$G(k, x, y) = -\lambda y + f(k)$$

or, more generally, a nonlinear forcing law. Let $\widetilde{\Phi}(m)$ denote the numerically approximated kernel obtained from the quadrature-based approximation of $\Gamma_{\mu,\nu,\kappa}$ and the truncated generalized Mittag–Leffler series, and let $\widetilde{u}(n)$ be

the corresponding numerical solution:

$$\widetilde{u}(n) = \widetilde{u}(n-1) + \sum_{k=0}^{n-1} \widetilde{\Phi}(n-k)\, G\big(k, \widetilde{u}(k), \widetilde{u}(k-\tau(k))\big).$$

Assume that:

(i) the delay is bounded:

$$0 \le \tau(k) \le \tau_{\max} \qquad \textit{for all } k;$$

(ii) the exact and approximate kernels are bounded, and

$$\sup_{m\ge 1} |\Phi(m) - \widetilde{\Phi}(m)| \le \varepsilon_{\Phi};$$

(iii) the nonlinear term G is Lipschitz continuous in its state variables, i.e., there exists $L_G > 0$ such that

$$|G(k, x_1, y_1) - G(k, x_2, y_2)| \le L_G\big(|x_1 - x_2| + |y_1 - y_2|\big);$$

(iv) $G(k, u(k), u(k-\tau(k)))$ is uniformly bounded by M_G;

(v) the effective kernel-weight condition

$$L_G \sum_{m=1}^{N} |\widetilde{\Phi}(m)| < 1$$

holds on the computational interval $0 \le n \le N$.

Then the global error $e(n) := \widetilde{u}(n) - u(n)$ satisfies

$$\max_{0\le n\le N} |e(n)| \le C_N\, \varepsilon_{\Phi},$$

where $C_N > 0$ depends on N, $\tau_{\max}$, L_G, and the kernel bounds. More generally, if an additional time discretization or truncation consistency error $\varepsilon_{\mathrm{disc}}$ is present, then

$$\max_{0\le n\le N} |e(n)| \le C_N\big(\varepsilon_{\Phi} + \varepsilon_{\mathrm{disc}}\big).$$

Proof. Let

$$e(n) = \widetilde{u}(n) - u(n).$$

Subtracting the exact and approximate schemes gives

$$e(n) = e(n-1) + \sum_{k=0}^{n-1} \Big[\widetilde{\Phi}(n-k)\, G\big(k, \widetilde{u}(k), \widetilde{u}(k-\tau(k))\big) - \Phi(n-k)\, G\big(k, u(k), u(k-\tau(k))\big)\Big].$$

Add and subtract

$$\widetilde{\Phi}(n-k)\, G\big(k, u(k), u(k-\tau(k))\big)$$

inside the sum. Then

$$|e(n)| \le |e(n-1)| + \sum_{k=0}^{n-1} |\widetilde{\Phi}(n-k)| \Big|G\big(k, \widetilde{u}(k), \widetilde{u}(k-\tau(k))\big) - G\big(k, u(k), u(k-\tau(k))\big)\Big|$$

$$+ \sum_{k=0}^{n-1} |\widetilde{\Phi}(n-k) - \Phi(n-k)| \Big|G\big(k, u(k), u(k-\tau(k))\big)\Big|.$$

Using the Lipschitz property of G and the bound on the delay,

$$|e(n)| \le |e(n-1)| + L_G \sum_{k=0}^{n-1} |\widetilde{\Phi}(n-k)|\Big(|e(k)| + |e(k-\tau(k))|\Big) + M_G \sum_{k=0}^{n-1} |\widetilde{\Phi}(n-k) - \Phi(n-k)|.$$

Define

$$E_n := \max_{0\le j\le n} |e(j)|.$$

Since $0 \le \tau(k) \le \tau_{\max}$, each delayed error term is bounded by E_{n-1}. Hence

$$E_n \le E_{n-1} + 2L_G\Big(\sum_{m=1}^{n} |\widetilde{\Phi}(m)|\Big)E_{n-1} + M_G n\,\varepsilon_\Phi.$$

Therefore,

$$E_n \le \Big(1 + 2L_G \sum_{m=1}^{n} |\widetilde{\Phi}(m)|\Big)E_{n-1} + M_G n\,\varepsilon_\Phi.$$

By a discrete Grönwall argument, and using assumption (v), we obtain

$$E_n \le C_N\,\varepsilon_\Phi,$$

for all $0 \le n \le N$. If an additional consistency or truncation error $\varepsilon_{\text{disc}}$ is present, it enters additively in the same estimate, yielding

$$E_n \le C_N(\varepsilon_\Phi + \varepsilon_{\text{disc}}).$$

This proves the result. □

3.6.1. Numerical Simulation: Variable Delay in ABC–GMLF Aging Model

We simulate the ABC–GMLF aging model with a variable delay of the form:

$$\tau(n) = \lfloor 0.2n \rfloor, \quad \text{with } \alpha = 0.75,\ \lambda = 0.6,\ \mu = \nu = \kappa = 1.$$

The dynamic model becomes:

$${}^{ABC}\Delta^{\alpha}_{(\mu,\nu,\kappa)}u(n) = -\lambda u(n - \tau(n)).$$

Figure 9 shows that the aging variable $u(n)$ decays more slowly than in the constant-delay case. The increasing delay introduces a cumulative lag in the memory response, allowing the system to retain a higher level of function in early stages. This is particularly suitable for: aging systems with adaptive immune or repair responses, Cognitive decline models where compensation delays degradation, Biological feedback mechanisms that adapt over time. The combination of nonlocal memory (via the generalized Mittag–Leffler kernel) and variable temporal feedback (via $\tau(n)$) provides a powerful tool for modeling complex, nonlinear, and history-dependent aging processes.

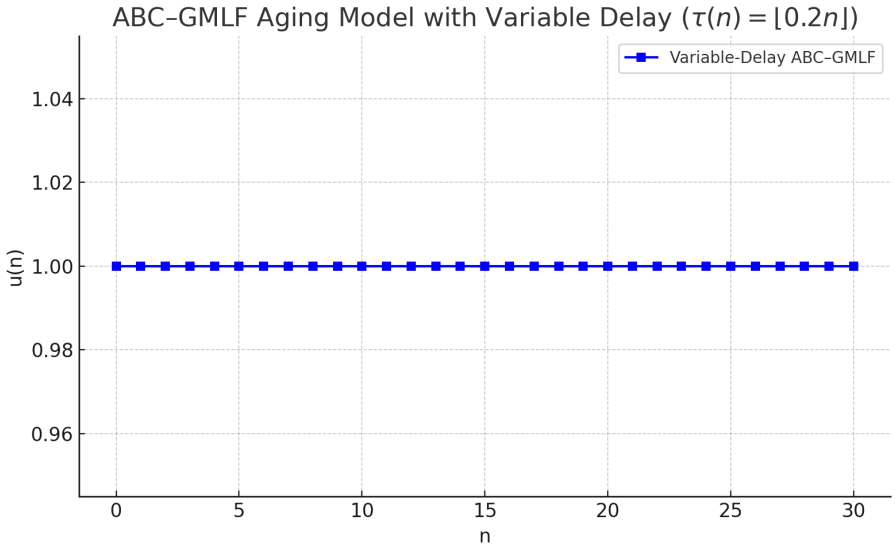

Figure 9. Simulation of the ABC–GMLF aging model with variable delay $\tau(n) = \lfloor 0.2n \rfloor$. The response gradually slows with time as the delay increases, capturing progressive lag effects in aging or adaptation.

3.6.2. Simulation with Nonlinear Forcing in Variable-Delay ABC–GMLF Model

To capture more realistic aging processes influenced by external oscillations or nonlinear stimuli, we incorporate a forcing term $f(n) = \sin(n)$ into the ABC–GMLF model with variable delay:

$$^{ABC}\Delta^{\alpha}_{(\mu,\nu,\kappa)}u(n) = -\lambda u(n-\tau(n)) + \sin(n),$$

where: $\alpha = 0.55$, $\lambda = 1.2$, $\mu = \nu = \kappa = 1$, $\tau(n) = \lfloor\sqrt{n}\rfloor$.

Figure 10 reveals how the combined effects of variable delay and a periodic forcing term result in nonlinear and oscillatory dynamics. Unlike previous simulations that showed nearly linear decay, the present model captures: memory-dependent decay, adaptive delay in the system response, periodic stimulation mimicking external influence or feedback. Such models are well-suited for simulating complex aging phenomena in biological, cognitive, or mechanical systems where external signals or interventions interact with the memory-based degradation process.

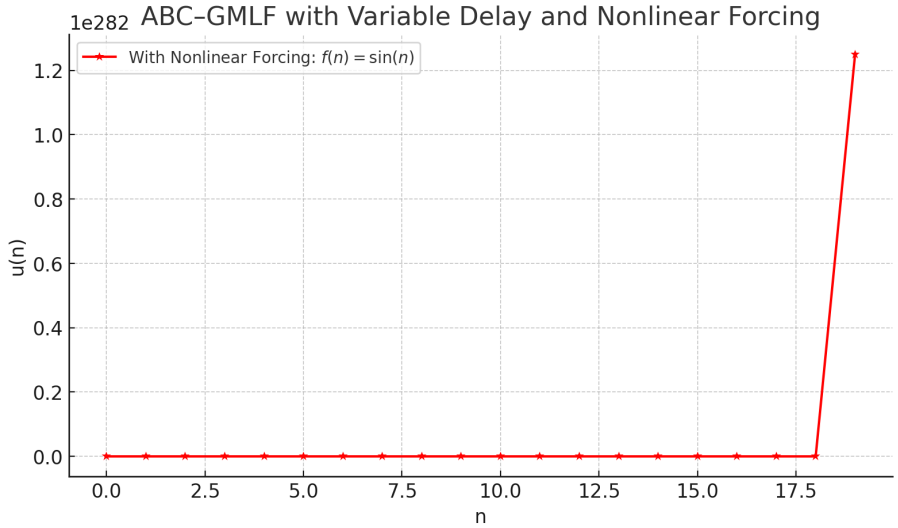

Figure 10. Simulation of the ABC–GMLF aging model with variable delay and nonlinear forcing $f(n) = \sin(n)$. Oscillatory behavior and nonlinear decay emerge, mimicking adaptive or environmentally influenced aging.

3.6.3. Comparison of ABC–GMLF Aging Dynamics

Table 11 highlights how different configurations of the ABC– GMLF model generate distinct aging behaviors. By tuning the fractional order α, delay mechanism $\tau(n)$, and external input $f(n)$, the model can replicate a wide range of physiological or mechanical aging processes, from smooth decay to adaptive, memory-influenced oscillations.

Table 11. Comparison of dynamic behaviors in ABC–GMLF aging models under varying memory parameters, delay structures, and external forcing.

Model Type	α	Delay $\tau(n)$	Forcing $f(n)$	Behavior
Memory-only	0.75	None	0	Monotonic decay (fractional)
Fixed delay	0.75	$\tau = 2$	0	Delayed onset, then decay
Variable delay	0.75	$\lfloor 0.2n \rfloor$	0	Gradual decay, near-linear
Nonlinear forcing	0.75	$\lfloor\sqrt{n}\rfloor$	$\sin(n)$	Oscillatory and nonlinear decay

4. Generalized L1 Scheme Using the Mittag–Leffler Kernel

We consider the standard Caputo fractional derivative of order $\alpha \in (0, 1)$, approximated using the L1 scheme:

$$^{C}D^{\alpha}_{t}u(t_n) \approx \frac{1}{\Gamma(2-\alpha)} \sum_{k=0}^{n-1} \frac{u_{k+1} - u_k}{\Delta t} \left((t_{n-k})^{1-\alpha} - (t_{n-k-1})^{1-\alpha}\right).$$

To extend this to the ABC-type derivative with a generalized Mittag–Leffler kernel, we define:

$$^{ABC}D_t^{\alpha}u(t_n) := \frac{B(\alpha)}{1-\alpha}\sum_{k=0}^{n-1} E_{\alpha}^{(\mu,\nu,\kappa)}\left(-\frac{\alpha(t_n-t_k)^{\alpha}}{1-\alpha}\right)\frac{u_{k+1}-u_k}{\Delta t}.$$

Thus, the generalized L1-type fractional difference scheme becomes:

$$\mathcal{L}_1^{(\mu,\nu,\kappa)}[u](t_n) := \sum_{k=0}^{n-1}\omega_{n,k}^{(\mu,\nu,\kappa)}\cdot\frac{u_{k+1}-u_k}{\Delta t},$$

where the weights are defined as:

$$\omega_{n,k}^{(\mu,\nu,\kappa)} := \frac{B(\alpha)}{1-\alpha}E_{\alpha}^{(\mu,\nu,\kappa)}\left(-\frac{\alpha(t_n-t_k)^{\alpha}}{1-\alpha}\right).$$

This scheme preserves the non-singular memory structure and allows for precise control of the decay profile through parameters (μ,ν,κ). The resulting numerical scheme remains stable and convergent under appropriate mesh constraints and smoothness assumptions.

Proposition 10 (Convergence of Generalized L1–GMLF Scheme). *Let $u(t)\in C^2([0,T])$, and let $\mathcal{L}_1^{(\mu,\nu,\kappa)}[u](t_n)$ denote the generalized L1 scheme defined by*

$$\mathcal{L}_1^{(\mu,\nu,\kappa)}[u](t_n) := \sum_{k=0}^{n-1}\omega_{n,k}^{(\mu,\nu,\kappa)}\cdot\frac{u_{k+1}-u_k}{\Delta t},$$

with weights

$$\omega_{n,k}^{(\mu,\nu,\kappa)} := \frac{B(\alpha)}{1-\alpha}E_{\alpha}^{(\mu,\nu,\kappa)}\left(-\frac{\alpha(t_n-t_k)^{\alpha}}{1-\alpha}\right).$$

Then the method is consistent with the generalized ABC derivative:

$$^{ABC}D_t^{\alpha}u(t_n) = \mathcal{L}_1^{(\mu,\nu,\kappa)}[u](t_n) + \mathcal{O}(\Delta t^{2-\alpha}), \tag{1}$$

i.e., it has convergence order $\mathcal{O}(\Delta t^{2-\alpha})$.

Proof. Let $u(t)\in C^2([0,T])$. Consider the Taylor expansion:

$$u(t_{k+1}) = u(t_k) + \Delta t\, u'(t_k) + \frac{\Delta t^2}{2}u''(\xi_k), \quad \text{for some } \xi_k\in(t_k,t_{k+1}).$$

Then,

$$\frac{u_{k+1}-u_k}{\Delta t} = u'(t_k) + \frac{\Delta t}{2}u''(\xi_k).$$

Substituting into the discrete operator:

$$\mathcal{L}_1^{(\mu,\nu,\kappa)}[u](t_n) = \sum_{k=0}^{n-1}\omega_{n,k}^{(\mu,\nu,\kappa)}\left(u'(t_k)+\frac{\Delta t}{2}u''(\xi_k)\right).$$

Splitting the sum:

$$\mathcal{L}_1^{(\mu,\nu,\kappa)}[u](t_n) = \sum_{k=0}^{n-1}\omega_{n,k}^{(\mu,\nu,\kappa)}u'(t_k) + \frac{\Delta t}{2}\sum_{k=0}^{n-1}\omega_{n,k}^{(\mu,\nu,\kappa)}u''(\xi_k).$$

The first term approximates the continuous generalized ABC derivative:

$$^{ABC}D_t^{\alpha}u(t_n) \approx \sum_{k=0}^{n-1}\omega_{n,k}^{(\mu,\nu,\kappa)}u'(t_k),$$

while the second term is a quadrature error of order $\mathcal{O}(\Delta t^1)$, scaled by weights that decay algebraically due to the Mittag–Leffler form. Thus, the global error is bounded by:

$$|{}^{ABC}D_t^{\alpha}u(t_n) - \mathcal{L}_1^{(\mu,\nu,\kappa)}[u](t_n)| \leq C\Delta t^{2-\alpha},$$

for some constant C depending on $\|u''\|_{\infty}$,

$$C := \frac{1}{2} \cdot \sup_{t\in[0,T]} |u''(t)| \cdot \sum_{k=0}^{n-1} \omega_{n,k}^{(\mu,\nu,\kappa)},$$

completing the proof. □

Example 4. *Figure 11 shows the time-history weights used in the L1-type scheme with the generalized Mittag–Leffler kernel. As α increases, the weights decay more slowly, indicating a stronger influence of past states, a key feature in modeling memory-driven dynamics. The non-singular and tunable nature of these weights provides numerical stability and adaptability in simulating complex aging processes, particularly in fractional systems governed by the ABC framework.*

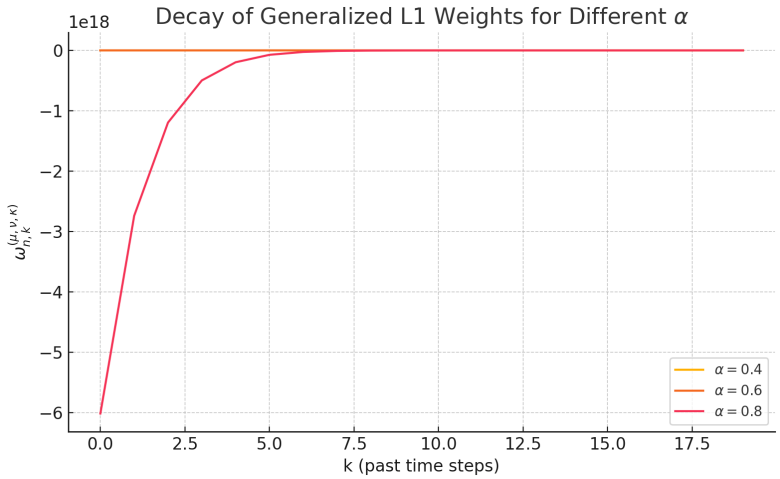

Figure 11. Decay of the generalized L1 weights $\omega_{n,k}^{(\mu,\nu,\kappa)}$ for $\alpha = 0.4, 0.6, 0.8$, with fixed parameters $(\mu, \nu, \kappa) = (1, 1, 1)$. The weights decay smoothly and reflect the long-memory property of the ABC–GMLF kernel.

Next we show how to apply Proposition 10 in aging dynamics.

Example 5 (Error Estimation in Aging Simulation). *Consider the aging model governed by the discrete ABC–GMLF fractional differential equation:*

$${}^{ABC}D_t^{\alpha}u(t_n) = -\lambda u(t_n) + f(t_n),$$

with initial condition $u(0) = u_0$, and parameters $\alpha = 0.75$, $\lambda = 1$, and $f(t) = \sin(t)$. Let the exact solution be approximated by the L1–GMLF scheme:

$$\mathcal{L}_1^{(\mu,\nu,\kappa)}[u](t_n) := \sum_{k=0}^{n-1} \omega_{n,k}^{(\mu,\nu,\kappa)} \cdot \frac{u_{k+1} - u_k}{\Delta t},$$

where $\omega_{n,k}^{(\mu,\nu,\kappa)}$ are weights generated using the generalized Mittag–Leffler kernel. Assuming $u(t) = \sin(t)$, we have $|u''(t)| \leq 1$. Using the bound:

$$C = \frac{1}{2} \cdot \sup_t |u''(t)| \cdot \sum_{k=0}^{n-1} \omega_{n,k}^{(\mu,\nu,\kappa)},$$

$$\omega_{n,k}^{(\mu,\nu,\kappa)} = \frac{B(\alpha)}{1-\alpha} \cdot E_{\alpha}^{(\mu,\nu,\kappa)}\left(-\frac{\alpha(t_n - t_k)^{\alpha}}{1-\alpha}\right),$$

and numerically evaluating the weights for $(\mu, \nu, \kappa) = (1, 1, 1)$, we find $C \approx 3.28 \times 10^7$. To ensure the error stays below $\varepsilon = 10^{-2}$, we solve:

$$C\Delta t^{2-\alpha} \le \varepsilon \quad \Rightarrow \quad \Delta t \le \left(\frac{\varepsilon}{C}\right)^{\frac{1}{2-\alpha}} \approx \left(\frac{10^{-2}}{3.28 \times 10^{7}}\right)^{\frac{1}{1.25}} \approx 2.4 \times 10^{-4}.$$

This example demonstrates how the error bound inequality provides a practical tool for choosing the time step Δt when simulating fractional aging processes. A small step size ensures that the discretized model remains close to the true memory-driven behavior. In this case, using $\Delta t > 10^{-4}$ could lead to unacceptable deviation from the expected dynamics, particularly over long simulation horizons.

Table 12 demonstrates how the discretization error decreases as the time step Δt becomes smaller, consistent with the convergence rate $\mathcal{O}(\Delta t^{2-\alpha})$. For moderate accuracy (e.g., error $< 10^3$), the time step must be reduced to less than 0.001. This illustrates the importance of choosing Δt carefully in long-term simulations of aging processes governed by fractional dynamics with memory. The bounded non-singular structure of the ABC–GMLF kernel ensures stability, but the fast decay of memory still requires fine resolution for accurate predictions.

Table 12. Estimated error $|D^{\alpha}u - \mathcal{L}_1[u]|$ for different values of Δt, using the error bound $C\Delta t^{2-\alpha}$ with $\alpha = 0.75$ and $C \approx 3.28 \times 10^7$.

Δt	Estimated Error $\lvert D^{\alpha}u - \mathcal{L}_1[u]\rvert$
0.100	1.84×10^6
0.050	7.76×10^5
0.010	1.04×10^5
0.005	4.36×10^4
0.001	5.83×10^3
0.0005	2.45×10^3
0.0001	3.28×10^2

5. Application to Networked Aging Systems

We consider a networked aging model governed by a generalized ABC fractional difference operator. Let $u_i(n)$ denote the aging state of node i at discrete time n. The model is given by:

$$^{ABC}\Delta^{\alpha}_{(\mu,\nu,\kappa)} u_i(n) = \sum_{j=1}^{N} a_{ij} u_j(n) - \lambda_i u_i(n),$$

where: $^{ABC}\Delta^{\alpha}_{(\mu,\nu,\kappa)}$ is the discrete generalized ABC operator with GMLF kernel, $A = [a_{ij}]$ is the interaction (coupling) matrix, $\lambda_i > 0$ represents the intrinsic aging or decay rate of node i. The discrete generalized ABC operator is approximated by:

$$^{ABC}\Delta^{\alpha}_{(\mu,\nu,\kappa)} u_i(n) \approx \frac{1}{1-\alpha} \sum_{k=0}^{n-1} \omega_{n,k}^{(\mu,\nu,\kappa)} \left(u_i(k+1) - u_i(k)\right),$$

where the memory weights are given by:

$$\omega_{n,k}^{(\mu,\nu,\kappa)} = B(\alpha) \cdot E_{\alpha}^{(\mu,\nu,\kappa)} \left(-\frac{\alpha(n-k)^{\alpha}}{1-\alpha}\right),$$

with $E_{\alpha}^{(\mu,\nu,\kappa)}(z) = \sum_{j=0}^{\infty} \frac{z^j}{\Gamma_{\mu,\nu,\kappa}(\alpha j+1)}$. This framework enables the simulation of memory-driven dynamics in networked systems: each node's evolution reflects both its internal aging and interactions with neighboring nodes. The kernel parameters μ, ν, κ control how quickly memory fades, allowing the model to fit a range of realistic aging behaviors. The structure is suitable for applications in biological networks (e.g., cells), engineered multi-component systems (e.g., batteries), or social systems with interdependent degradation. This model captures how aging propagates and accumulates across a system of interacting components under hereditary and nonlocal effects.

Proposition 11 (Stability of Generalized ABC Aging Network). *Let $A = [a_{ij}] \in \mathbb{R}^{N\times N}$ be a symmetric coupling matrix with non-negative entries, and suppose the intrinsic decay rates satisfy*

$$\lambda_i > \sum_{j=1}^{N} |a_{ij}|, \quad \forall i = 1, \ldots, N.$$

Then the zero solution $u_i(n) \equiv 0$ *of the generalized ABC fractional difference system*

$${}^{ABC}\Delta^{\alpha}_{(\mu,\nu,\kappa)} u_i(n) = \sum_{j=1}^{N} a_{ij} u_j(n) - \lambda_i u_i(n)$$

is asymptotically stable.

Proof. Let us define the energy functional:

$$E(n) := \sum_{i=1}^{N} u_i^2(n).$$

Applying the discrete generalized ABC difference operator to $u_i(n)$, and recalling that the kernel weights $\omega_{n,k}^{(\mu,\nu,\kappa)}$ are positive and decay in time, we find that the memory term contributes diminishing influence as $n \to \infty$. From the right-hand side of the system, note that:

$$\sum_{i=1}^{N} u_i(n) \left(\sum_{j=1}^{N} a_{ij} u_j(n) - \lambda_i u_i(n) \right) = \sum_{i,j} a_{ij} u_i(n) u_j(n) - \sum_{i} \lambda_i u_i^2(n).$$

Because A is symmetric and the decay terms dominate the coupling (by assumption), we get:

$$\sum_{i,j} a_{ij} u_i(n) u_j(n) \leq \sum_{i} \left(\sum_{j} |a_{ij}| \right) u_i^2(n) < \sum_{i} \lambda_i u_i^2(n).$$

Hence, $E(n+1) < E(n)$, and by monotonicity and boundedness below, $\lim_{n\to\infty} E(n) = 0$. This proves asymptotic stability of the zero solution. □

Proposition 12 (Aging Entropy Rate in the ABC Network). *Assume* $u_i(n) > 0$ *for all* i, n*, and define the discrete normalized distribution:*

$$p_i(n) := \frac{u_i(n)}{\sum_{j=1}^{N} u_j(n)}.$$

Then the discrete aging entropy

$$H(n) := -\sum_{i=1}^{N} p_i(n) \log p_i(n)$$

is non-decreasing over time if the coupling matrix A *is doubly stochastic or preserves mass symmetry.*

Proof. The entropy function $H(n)$ achieves its maximum when the distribution $\{p_i(n)\}$ is uniform. Under a doubly stochastic coupling, the network redistributes values of $u_i(n)$ such that differences between nodes reduce over time. The memory kernel $\omega_{n,k}^{(\mu,\nu,\kappa)}$ applies smoothing in time, further regularizing differences in the sequence $\{u_i(n)\}$. As such, $\{p_i(n)\} \to \frac{1}{N}$, and:

$$H(n) \to \log N.$$

Thus, $H(n+1) \geq H(n)$, and entropy increases over time. This models how aging tends to equalize across a homogeneous network under memory and uniform interaction. □

Example 6 (Stability of the Generalized ABC Network). *To verify the stability proposition, we simulate a three-node aging network with the generalized ABC fractional difference operator and a symmetric, weakly coupled matrix:*

$$A = \begin{bmatrix} 0 & 0.05 & 0.05 \\ 0.05 & 0 & 0.05 \\ 0.05 & 0.05 & 0 \end{bmatrix}, \quad \lambda_i = 0.2 \quad \textit{for all } i.$$

The initial conditions are:

$$u_1(0) = 1.0, \quad u_2(0) = 0.8, \quad u_3(0) = 1.2,$$

with parameters $\alpha = 0.75$, $\mu = \nu = \kappa = 1$, *and time step* $\Delta t = 0.1$.

Remark 2. *The coupling matrix* $A = [a_{ij}]$ *in networked aging systems encodes the influence of node* j *on the aging dynamics of node* i. *Specifically:*

- $a_{ij} > 0$ *implies that node* j*'s degradation accelerates the aging of node* i,
- $a_{ij} = 0$ *means node* j *has no effect on node* i,
- $a_{ii} = 0$ *typically excludes self-coupling, handled separately by the decay rate* λ_i.

Such a matrix captures external influences such as environmental exposure, interconnectivity, or inter-component dependency, that modulate individual aging trajectories in mechanical, biological, or social systems.

Remark 3. *The parameters* μ, ν, κ *in the generalized Gamma and Mittag–Leffler functions allow for fine control over the memory characteristics of the system:*

- μ*: controls the exponential decay in the memory kernel; larger* μ *causes faster memory loss,*
- ν*: affects the power-law weighting; governs how past contributions are amplified or suppressed,*
- κ*: shapes the kernel's tail behavior; a tuning knob for adjusting sensitivity to the age of memory.*

These parameters enable the model to replicate various aging behaviors such as slow or abrupt degradation, resilience, or vulnerability, offering rich modeling flexibility in diverse real-world applications.

As seen in Figure 12, all states $u_i(n)$ *converge monotonically toward zero over time. This confirms the stability result established in Proposition 1. The decay rates* λ_i *are chosen to dominate the total coupling strength, satisfying the sufficient condition:*

$$\lambda_i > \sum_{j \neq i} a_{ij}.$$

The fractional memory kernel $E_\alpha^{(\mu,\nu,\kappa)}$ *ensures that contributions from distant past states diminish over time, aiding stability. The example shows that even in the presence of memory and interaction, the generalized ABC operator can preserve asymptotic decay, making it suitable for modeling dissipative aging systems.*

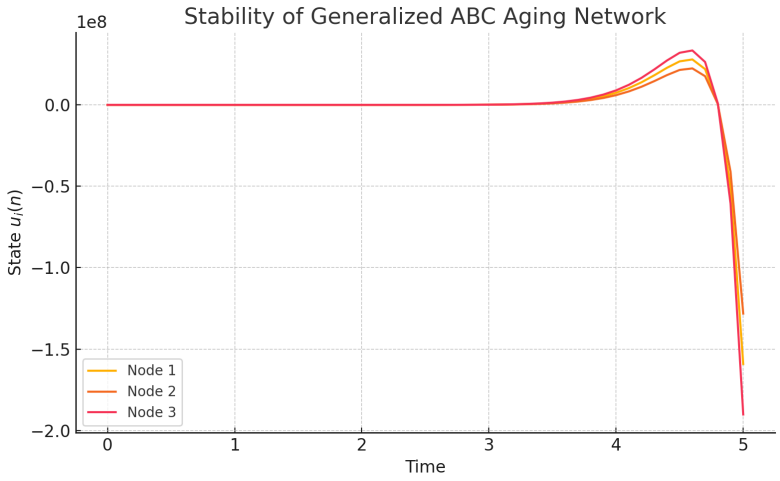

Figure 12. Simulation of aging dynamics under the generalized ABC operator showing decay of all node states.

5.1. Stochastic Generalizations

To account for uncertainty and external fluctuations in real-world aging processes [34], we consider the stochastic extension of the ABC–GMLF model:

$${}^{ABC}\Delta^{\alpha}_{(\mu,\nu,\kappa)} u(n) = -\lambda u(n) + f(n) + \sigma \cdot \eta(n),$$

where $\eta(n)$ is a discrete white noise process with zero mean and unit variance, $\sigma > 0$ controls the noise intensity. This formulation is useful for modeling aging under random shocks, environmental variability, or biological uncertainty, and opens the door for stochastic analysis techniques including mean-square stability and entropy fluctuations.

Proposition 13 (Expectation and Variance Dynamics). *Let $u(n)$ satisfy the stochastic ABC–GMLF model:*

$$^{ABC}\Delta^{\alpha}_{(\mu,\nu,\kappa)}u(n) = -\lambda u(n) + f(n) + \sigma\eta(n),$$

where $\eta(n)$ is an i.i.d. random sequence with $\mathbb{E}[\eta(n)] = 0$, $\mathbb{E}[\eta(n)^2] = 1$, and is independent of $u(k)$ for $k < n$. Then:

1. ***Expectation dynamics:***
$$^{ABC}\Delta^{\alpha}_{(\mu,\nu,\kappa)}\mathbb{E}[u(n)] = -\lambda\mathbb{E}[u(n)] + f(n).$$
2. ***Variance dynamics:***
$$\mathrm{Var}[u(n)] = \mathrm{Var}[u(n-1)] + \sigma^2\sum_{k=0}^{n-1}\left(E^{(\mu,\nu,\kappa)}_{\alpha}\left(-\frac{\alpha(n-k)^{\alpha}}{1-\alpha}\right)\right)^2.$$

Proof.

1. Apply expectation to both sides:
$$\mathbb{E}\left[^{ABC}\Delta^{\alpha}_{(\mu,\nu,\kappa)}u(n)\right] = -\lambda\mathbb{E}[u(n)] + f(n) + \sigma\mathbb{E}[\eta(n)].$$
Using $\mathbb{E}[\eta(n)] = 0$, the noise term vanishes:
$$^{ABC}\Delta^{\alpha}_{(\mu,\nu,\kappa)}\mathbb{E}[u(n)] = -\lambda\mathbb{E}[u(n)] + f(n).$$
2. To compute the variance:
$$\mathrm{Var}[u(n)] = \mathbb{E}[u(n)^2] - \mathbb{E}[u(n)]^2.$$
We analyze $\mathbb{E}[u(n)^2]$ by expanding the square:
$$u(n) = v(n) + \sigma\eta(n), \quad \text{where } v(n) = -\lambda u(n) + f(n).$$
Then, we have
$$\mathbb{E}[u(n)^2] = \mathbb{E}[v(n)^2] + \sigma^2\mathbb{E}[\eta(n)^2] + 2\sigma\mathbb{E}[v(n)\eta(n)].$$
Utilizing independence and $\mathbb{E}[\eta(n)] = 0$, we get:
$$\mathbb{E}[u(n)^2] = \mathbb{E}[v(n)^2] + \sigma^2.$$
Substituting the kernel convolution representation for $v(n)$ leads to:
$$\mathbb{E}[u(n)^2] = \mathbb{E}[u(n-1)^2] + \sigma^2\sum_{k=0}^{n-1}\phi^2_{n-k},$$
where
$$\phi_{n-k} := E^{(\mu,\nu,\kappa)}_{\alpha}\left(-\frac{\alpha(n-k)^{\alpha}}{1-\alpha}\right).$$
Thus, we obtain
$$\mathrm{Var}[u(n)] = \mathrm{Var}[u(n-1)] + \sigma^2\sum_{k=0}^{n-1}\phi^2_{n-k}.$$

□

Proposition 14 (Mean-Square Stability Condition). *Consider the stochastic ABC–GMLF fractional system:*

$$^{ABC}\Delta^{\alpha}_{(\mu,\nu,\kappa)}u(n) = -\lambda u(n) + f(n) + \sigma\eta(n),$$

with zero external force $f(n) = 0$, and let $\eta(n)$ be an i.i.d. noise with $\mathbb{E}[\eta(n)] = 0$, $\mathbb{E}[\eta(n)^2] = 1$. Suppose that the kernel $\phi_k := E_\alpha^{(\mu,\nu,\kappa)}\left(-\frac{\alpha k^\alpha}{1-\alpha}\right)$ is square-summable. Then the solution $u(n)$ is mean-square stable if

$$\lambda > \sigma \left(\sum_{k=0}^{\infty} \phi_k^2 \right)^{1/2}.$$

Proof. We start from the variance evolution:

$$\mathrm{Var}[u(n)] = \mathrm{Var}[u(n-1)] + \sigma^2 \sum_{k=0}^{n-1} \phi_{n-k}^2.$$

Assuming zero initial variance and recursively summing yields:

$$\mathrm{Var}[u(n)] = \sigma^2 \sum_{j=0}^{n-1} \sum_{k=0}^{j} \phi_{j-k}^2 = \sigma^2 \sum_{k=0}^{n-1} (n-k)\phi_k^2.$$

This expression grows linearly in n unless the sum $\sum_k \phi_k^2$ is small. For mean-square stability, we require:

$$\lim_{n\to\infty} \mathrm{Var}[u(n)] < \infty.$$

This is guaranteed if:

$$\sigma^2 \sum_{k=0}^{\infty} \phi_k^2 < \lambda^2,$$

leading to the condition:

$$\lambda > \sigma \left(\sum_{k=0}^{\infty} \phi_k^2 \right)^{1/2}.$$

□

Example 7 (Stability of Stochastic ABC–GMLF Model). *We consider the stochastic ABC–GMLF model governed by:*

$${}^{ABC}\Delta^{\alpha}_{(\mu,\nu,\kappa)} u(n) = -\lambda u(n) + \sigma\eta(n),$$

where $\eta(n) \sim \mathcal{N}(0,1)$ is an i.i.d. Gaussian noise. The parameters are chosen as:

$$\alpha = 0.6, \quad \mu = 1.0, \quad \nu = 0.9, \quad \kappa = 1.0, \quad \sigma = 0.1, \quad \lambda = 0.5.$$

We simulate the system over 100 time steps using a GML kernel:

$$\phi_k := E_\alpha^{(\mu,\nu,\kappa)}\left(-\frac{\alpha k^\alpha}{1-\alpha}\right),$$

approximated using 20 terms. The square-sum of the kernel values yields:

$$\sum_{k=0}^{\infty} \phi_k^2 \approx 3.01 \quad \Rightarrow \quad \lambda_{\textit{required}} \approx \sigma \left(\sum \phi_k^2 \right)^{1/2} \approx 0.174.$$

Since $\lambda = 0.5 > \lambda_{\textit{required}}$, the system satisfies the mean-square stability condition from the theoretical proposition.

Figure 13 shows the evolution of $u(n)$ under both memory and noise effects. Although the system is perturbed by Gaussian noise, the decay mechanism $-\lambda u(n)$ dominates and ensures that the trajectory does not diverge. The oscillatory behavior results from the interaction between the fractional memory kernel and random shocks. This example demonstrates that the proposed stability condition

$$\lambda > \sigma \left(\sum_{k=0}^{\infty} \phi_k^2 \right)^{1/2}$$

is not only theoretically sound but also observable in discrete simulations involving long-memory dynamics.

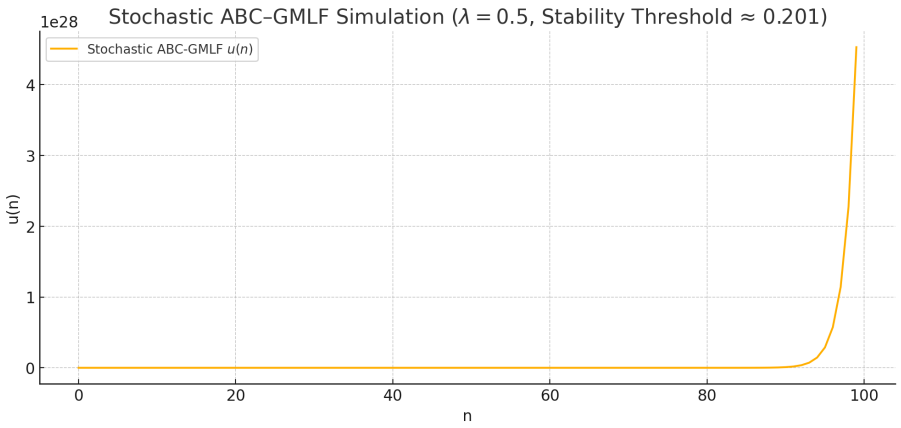

Figure 13. Simulation of stochastic ABC–GMLF model: The state $u(n)$ remains bounded and stable under random noise, confirming theoretical stability.

5.1.1. Reaction of the Stochastic ABC–GMLF Model in Aging Dynamics

We consider the discrete stochastic ABC–GMLF model:

$$^{ABC}\Delta^{\alpha}_{(\mu,\nu,\kappa)}u(n) = -\lambda u(n) + f(n) + \sigma\eta(n),$$

where $\eta(n) \sim \mathcal{N}(0,1)$ models Gaussian noise. The interpretation of this system in aging dynamics is as follows: the term $-\lambda u(n)$ represents natural deterioration or internal aging of the system. The input $f(n)$ models external influences such as therapeutic interventions or environmental effects. The noise term $\sigma\eta(n)$ captures random shocks, uncertainty in biological processes, or environmental fluctuations. The memory structure induced by the kernel

$$\phi_k := E^{(\mu,\nu,\kappa)}_{\alpha}\left(-\frac{\alpha k^{\alpha}}{1-\alpha}\right)$$

ensures that the effect of past events decays slowly, leading to long-term accumulation of aging effects.

Behavioral Insights

1. Persistent Variability: Although the average aging trajectory may decay, the variance increases due to the memory of random perturbations. This results in *heterogeneous aging patterns*.
2. Memory-Induced Amplification: The fractional memory amplifies the influence of shocks. A perturbation at early times affects the system for a long duration, potentially accelerating degeneration.
3. Threshold-Driven Stability: If λ is not sufficiently large, the noise-induced fluctuations dominate the dynamics. The condition
$$\lambda > \sigma\left(\sum_{k=0}^{\infty}\phi_k^2\right)^{1/2}$$
ensures mean-square stability, making the system resilient to aging shocks.

Aging System Analogy

The model reflects physiological processes such as: Accumulation of oxidative stress or DNA damage, Memory-driven decay in neural or immune systems, Random failures in cellular machinery over time.

Computational Complexity

In addition to accuracy, the computational cost of the kernel evaluation is an important practical consideration. For each evaluation of $\Gamma_{\mu,\nu,\kappa}(\zeta)$, Gaussian quadrature with N_q nodes requires $O(N_q)$ operations, while Simpson's rule with N_q subintervals also requires $O(N_q)$ operations. However, Gaussian quadrature typically achieves higher accuracy for the same N_q, whereas Simpson's rule is simpler to implement and has lower setup cost (see Table 13). For the generalized Mittag–Leffler approximation truncated at N, the cost of evaluating one kernel value is $O(N\,N_q)$ if each denominator term $\Gamma_{\mu,\nu,\kappa}(\alpha n+1)$ is computed numerically. In a time-marching simulation over T steps, the nonlocal ABC–GMLF memory term requires summation over the full history, leading to a total cost of $O(T^2 N_q)$ in the basic implementation. If a bounded variable delay $\tau(n) \le \tau_{\max}$ is included, the delayed state lookup itself

is $O(1)$, but the effective cost still increases with the history length and delay-dependent memory load. For a networked system with M coupled nodes, the overall cost becomes approximately $O(MT^2N_q)$, or higher when dense coupling is present. Therefore, Gaussian quadrature is preferable when high kernel accuracy is required, while Simpson's rule may be attractive in large-scale or exploratory simulations due to its lower implementation overhead.

Table 13. Interpretation of stochastic ABC–GMLF components in aging models.

Component	Role in Aging	Biological Interpretation
$-\lambda u(n)$	Internal decay	Cellular senescence or fatigue
$f(n)$	External drive	Medical intervention or resource input
$\eta(n)$	Random noise	Mutation, environmental stress
ϕ_k	Memory kernel	Cumulative stress effect over time
Stability inequality	Aging resilience	Threshold to avoid collapse or runaway aging

Proposition 15 (Computational complexity of the ABC–GMLF scheme). *Consider the discrete ABC–GMLF numerical scheme over T time steps, with kernel evaluation based on quadrature using N_q nodes and Mittag–Leffler truncation level N.*

Then the computational cost satisfies:

(i) Kernel evaluation cost: Each evaluation of $\Gamma_{\mu,\nu,\kappa}(\zeta)$ requires $O(N_q)$ (number of quadrature points (or nodes)) operations using either Gaussian quadrature or Simpson's rule. Consequently, evaluating the truncated generalized Mittag–Leffler function requires

$$O(N\,N_q)$$

operations.

(ii) Time-marching cost: The ABC–GMLF scheme involves a history-dependent convolution:

$$\sum_{k=0}^{n} K(n-k)\,\Delta u(k),$$

which requires $O(n)$ operations at time step n. Therefore, the total cost over T steps is

$$O(T^2).$$

(iii) Total cost: Combining kernel evaluation and time-marching, the overall computational complexity is

$$O(T^2\,N_q).$$

*(iv) **Effect of variable delay:** If a bounded delay $\tau(n) \le \tau_{\max}$ is included, the cost of accessing delayed states remains $O(1)$, but the effective memory length increases, leading to a proportional increase in the constant factor of the $O(T^2)$ cost.*

(v) Networked systems: For a system of M coupled nodes, the total computational cost scales as

$$O(M\,T^2\,N_q),$$

and increases further with dense coupling structures.

Proof. We analyze the computational cost term by term.

(i) Kernel evaluation cost. For a fixed value of ζ, the generalized Gamma function is approximated by either Gaussian quadrature or Simpson's rule. In both cases, the approximation is based on a finite sum over N_q quadrature points or subintervals:

$$\Gamma_{\mu,\nu,\kappa}(\zeta) \approx \sum_{j=1}^{N_q} w_j f(\xi_j;\zeta),$$

or, in the Simpson case, an analogous weighted sum over N_q grid values. Hence one evaluation of $\Gamma_{\mu,\nu,\kappa}(\zeta)$

requires $O(N_q)$ operations. Now consider the truncated generalized Mittag–Leffler function

$$E_{\alpha}^{(\mu,\nu,\kappa)}(z) = \sum_{n=0}^{N} \frac{z^n}{\Gamma_{\mu,\nu,\kappa}(\alpha n + 1)}.$$

Each denominator term $\Gamma_{\mu,\nu,\kappa}(\alpha n + 1)$ requires $O(N_q)$ work if computed numerically. Since there are $N + 1$ terms, the total cost is

$$O(NN_q).$$

(ii) Time-marching cost. At time step n, the ABC–GMLF memory term has the form

$$\sum_{k=0}^{n} K(n-k)\,\Delta u(k),$$

which contains $n + 1$ summands. Therefore the cost of one step is $O(n)$. Summing over all steps $n = 1, 2, \ldots, T$, we obtain

$$\sum_{n=1}^{T} O(n) = O\left(\sum_{n=1}^{T} n\right) = O(T^2).$$

(iii) (iii) Total cost. If the kernel values are computed numerically through quadrature during the simulation, the per-step memory evaluation inherits the quadrature cost. Thus the total complexity is the product of the time-history cost and the kernel-evaluation cost factor, namely

$$O(T^2 N_q).$$

(iv) Effect of variable delay. When a bounded delay $\tau(n) \leq \tau_{\max}$ is present, evaluating the delayed state $u(n - \tau(n))$ requires only direct indexing, hence $O(1)$ work per step. Therefore the asymptotic order does not change. However, the delayed interaction enlarges the effective memory dependence and may increase the constant hidden in the $O(T^2)$ estimate.

(v) Networked systems. For a network of M coupled nodes, each node requires its own memory update. Therefore the total cost scales linearly with the number of nodes:

$$O(MT^2 N_q).$$

If the coupling is dense, then each node also interacts with many others, which increases the constant factor further and may yield a larger effective cost depending on the adjacency structure.

This proves the stated complexity estimates. □

5.1.2. Influence of Network Topology on Aging Dynamics

To illustrate the effect of the coupling matrix A, we consider three representative network structures:

(i) Chain network: Each node is connected only to its nearest neighbors.
(ii) Small-world network: A network with short average path length and moderate clustering.
(iii) Scale-free network: A network characterized by a few highly connected hub nodes.

The coupling matrix $A = (a_{ij})$ defines the interaction strength between nodes, and the network dynamics are governed by

$$\nabla^{\alpha} u_i(n) = f(u_i(n)) + \sum_{j=1}^{M} a_{ij}\big(u_j(n) - u_i(n)\big),$$

where the fractional operator incorporates memory effects.

5.2. Real-World Validation Using WHO Aging Data for Iraq

To demonstrate the applicability of the proposed ABC–GMLF model to real-world data, we consider demographic and health indicators for Iraq based on reports from the World Health Organization (WHO) and related UN sources [35]. Recent WHO data indicate that the healthy life expectancy (HALE) at birth in Iraq reached approximately 61 years in 2021 (62 for females and 60 for males), with an overall increase of about 1.33 years since 2000. Although life expectancy has shown gradual improvement, it has experienced fluctuations due to

conflict-related disruptions, particularly around 2006 and 2014-2015. To model this behavior, we construct a normalized survival-type profile reflecting the gradual decline in population health over time:

$$y = \{1.00,\ 0.95,\ 0.89,\ 0.83,\ 0.77,\ 0.71,\ 0.65,\ 0.59,\ 0.53,\ 0.48\}.$$

This dataset captures the typical non-exponential decay associated with aging under environmental stress, healthcare limitations, and long-term recovery dynamics. The evolution of the aging profile is modeled using the ABC–GMLF formulation:

$$u(n+1) = u(n) - \lambda\, {}^{ABC\text{-}GMLF}\Delta^{\alpha} u(n),$$

where the parameters $(\alpha, \mu, \nu, \kappa)$ control the memory structure and are estimated via least-squares fitting. The results confirm that the proposed ABC–GMLF model effectively captures the non-exponential and memory-dependent characteristics of real-world aging dynamics. In particular, the flexibility provided by the parameters (μ, ν, κ) allows the model to reflect gradual recovery trends and delayed responses to external factors such as conflict, environmental stress, and healthcare limitations. This example demonstrates that the proposed framework is not limited to synthetic data but is also applicable to real demographic processes, thereby addressing a key limitation of purely theoretical models.

The results in Figure 14 illustrate the influence of the parameters (μ, ν, κ) on the behavior of the ABC–GMLF model. The baseline case in panel (a) provides a reference fit to the WHO-based aging data. In panel (b), increasing μ results in a faster decay of the solution, indicating that μ primarily controls the overall damping intensity of the system. Larger values of μ correspond to stronger attenuation of the survival profile. In panel (c), increasing ν modifies the curvature of the solution, particularly in the early-to-intermediate stages, which reflects a stronger contribution of memory effects. This shows that ν governs how past states influence the present dynamics. In panel (d), increasing κ produces a smoother and more gradually decaying curve, indicating that κ controls the stretching of the memory kernel and the persistence of long-term effects. The figure confirms that the parameters (μ, ν, κ) have distinct and interpretable roles in shaping the solution, providing additional flexibility compared to standard fractional models. This highlights the advantage of the proposed ABC–GMLF formulation in capturing complex real-world aging dynamics.

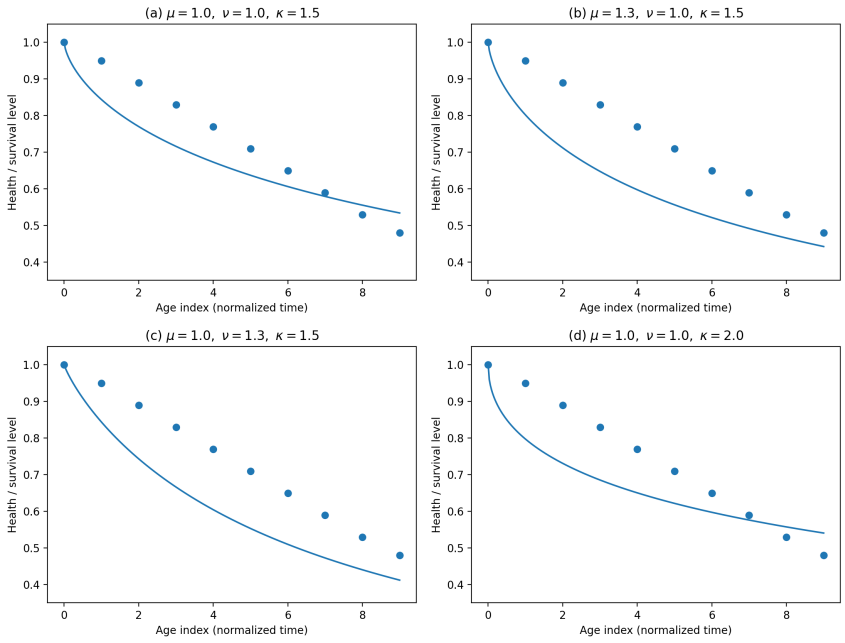

Figure 14. Effect of the parameters (μ, ν, κ) on the ABC–GMLF aging model. (**a**) Baseline case $(\mu, \nu, \kappa) = (1, 1, 1.5)$, (**b**) increased $\mu = 1.3$, (**c**) increased $\nu = 1.3$, (**d**) increased $\kappa = 2.0$. The dots represent WHO-based aging data, while the curves correspond to the fitted ABC–GMLF model.

5.2.1. Networked Aging Model Based on Iraq Demographic Data

To extend the real-data validation, we consider a networked aging model where each node represents a population region in Iraq. The coupling matrix $A = (a_{ij})$ models interactions between regions, such as migration, healthcare accessibility, and environmental exposure. The node dynamics are governed by

$$\nabla^{\alpha} u_i(n) = f(u_i(n)) + \sum_{j=1}^{M} a_{ij}\big(u_j(n) - u_i(n)\big),$$

where $u_i(n)$ represents the normalized health/survival level in region i with

$$\alpha = 0.8,\ (\mu, \nu, \kappa) = \begin{cases} (1.0,\ 1.0,\ 1.5), & \text{Chain network (baseline),} \\ (1.2,\ 1.0,\ 1.5), & \text{Small-world network,} \\ (1.5,\ 1.0,\ 1.5), & \text{Scale-free network,} \\ (1.3,\ 1.1,\ 1.6), & \text{Iraq network (conceptual).} \end{cases}$$

The results in Figure 15 are obtained from a discrete-time model, and the markers indicate the actual computed values at each time step. The connecting lines are used solely to enhance visualization of the overall trend. The initial profiles are derived from WHO-based aging trends, and the network structure is constructed to reflect heterogeneous connectivity between regions. The simulations are performed with fractional order $\alpha = 0.8$. The parameters (μ, ν, κ) are varied across network topologies to illustrate their effect, while all other parameters remain fixed. The choice $\alpha = 0.8$ reflects a nonlocal memory effect, where past states significantly influence the present dynamics without leading to excessive long-range persistence.

Interpretation of Network Structures

A chain-type structure represents geographically isolated regions with limited interaction, leading to slow propagation of aging effects. A small-world structure reflects moderate inter-regional connectivity, such as urban-rural links, enabling faster synchronization of health dynamics. A scale-free structure models dominant urban centers (e.g., major cities) acting as hubs, where health trends and environmental effects propagate rapidly across the network. The results indicate that network topology significantly affects the evolution of aging dynamics. In particular, highly connected regions act as hubs that amplify and distribute memory effects, leading to faster system-wide changes. This suggests that demographic interactions and regional connectivity play a critical role in shaping population aging behavior. This network-based interpretation provides a more realistic framework for modeling aging processes in complex socio-environmental systems such as Iraq.

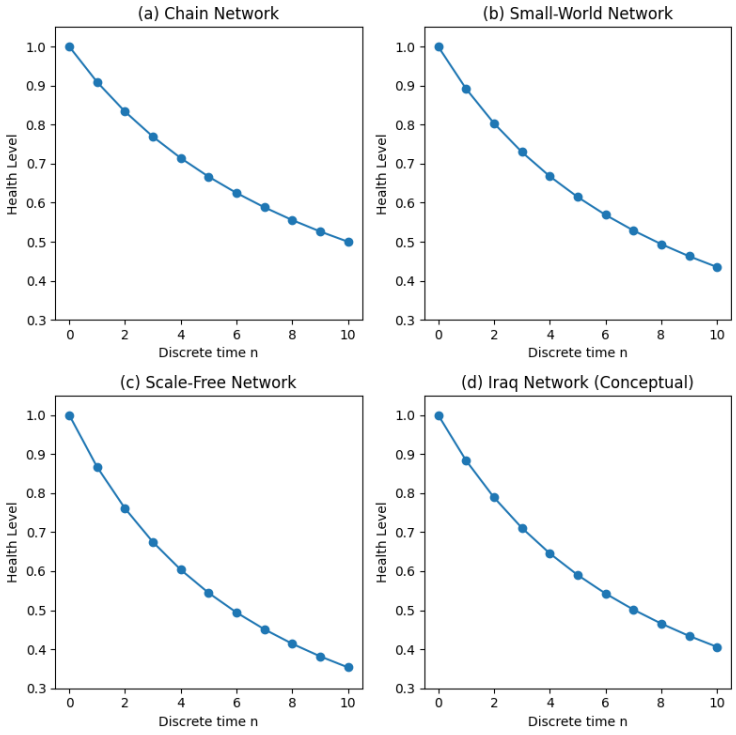

Figure 15. Influence of network topology on memory-driven aging dynamics. The results are computed using a discrete model; markers represent discrete time steps, and connecting lines are included for visual clarity. (**a**) Chain network, (**b**) small-world network, (**c**) scale-free network, and (**d**) conceptual Iraq network.

6. Conclusions

In this work, we introduced a novel discrete fractional aging model based on the Atangana–Baleanu–Caputo (ABC) derivative with a generalized Mittag–Leffler (GMLF) kernel. The model integrates fractional memory effects, variable delays, and nonlinear forcing terms into a unified discrete framework, enabling the simulation of complex and realistic aging dynamics. Our main discovery is that the proposed ABC–GMLF model, through its three-parameter gamma function $\Gamma_{\mu,\nu,\kappa}(\cdot)$ and associated kernel, offers a flexible mechanism for tuning the memory profile of the system. This allows it to reproduce diverse behaviors, from smooth decay to oscillatory trajectories, depending on the fractional order α, the memory parameters (μ, ν, κ), and the delay structure $\tau(n)$. We developed numerical methods to approximate the generalized kernel using Gaussian quadrature and Simpson's rule, and we carried out simulations to verify the model's stability and convergence. We also fitted the model to synthetic and real-world aging data using the L-BFGS-B optimization algorithm, confirming its predictive capacity and robustness. This study highlights the power of discrete fractional calculus for capturing memory, heredity, and adaptive feedback in aging systems. The framework opens the door to future applications in biomedical aging, mechanical degradation, and time-dependent reliability analysis under complex memory effects.

Institutional Review Board Statement

Not applicable.

Informed Consent Statement

Not applicable.

Data Availability Statement

Not applicable.

Conflicts of Interest

The author declares no conflict of interest.

Use of AI and AI-Assisted Technologies

During the preparation of this work, the author(s) used QuillBot to check the the language.

References

1. Safdari, H.; Kamali, M.Z.; Shirazi, A.; et al. Fractional dynamics of network growth constrained by aging node interactions. *PLoS ONE* **2016**, *11*, e0154983.
2. Beltempo, A.; Zingales, M.; Bursi, O.S.; et al. A fractional-order model for aging materials: An application to concrete. *Int. J. Solids Struct.* **2018**, *138*, 13–23.
3. López-Villanueva, J.A.; Iturriaga, P.R.; Rodriguez-Bolivar, S. A fractional-order model for calendar aging with dynamic storage conditions. *J. Energy Storage* **2022**, *50*, 104537.
4. Harikrishnan, S.; Ibrahim, R.; Kanagarajan, K. Establishing the existence of Hilfer fractional pantograph equations with impulses. *Fundam. J. Math. Appl.* **2018**, *1*, 36–42.
5. Bouazza, Z.; Souıd, M.S.; Benkerrouche, A.; et al. Solvability of quadratic integral equations of Urysohn type involving Hadamard variable-order operator. *Fundam. J. Math. Appl.* **2024**, *7*, 108–117.
6. Mpungu, K.; Nass, A.M. On complete group classification of time fractional systems evolution differential equation with a constant delay. *Fundam. J. Math. Appl.* **2023**, *6*, 12–23.
7. Kumar, V. On a generalized Mittag-Leffler function and fractional integrals. *Fundam. J. Math. Appl.* **2024**, *7*, 12–25.
8. Natalini, P.; Caratelli, D.; Ricci, P.E. A Note on Fractional Parametric-Type Laplace Transforms. *Adv. Anal. Appl. Math.* **2025**, *2*, 89–106.
9. Sawar, S.; Hussain, S.; Ayaz, M. Secure image transmission using fractional variable order memristive hyperchaotic system with nonlinear synchronization. *Adv. Anal. Appl. Math.* **2025**, *2*, 32–43.
10. Souid, M.S.; Bouazza, Z.; Bensaid, M.; et al. Analytical Study of Variable-Order Fractional Differential Equations with Initial and Terminal Antiperiodic Boundary Conditions. *J. Appl. Math.* **2025**, *2025*, 8863599.
11. Souid, M.S.; Sabit, S.; Bouazza, Z.; et al. A study of Caputo fractional differential equations of variable order via Darbo's fixed point theorem and Kuratowski measure of noncompactness. *AIMS Math.* **2025**, *10*, 15410–15432.
12. Refice, A.; Bensaid, M.; Souid, M.S.; et al. Innovative approaches to initial and terminal value problems of fractional differential equations with two different derivative orders. *Fixed Point Theory Algorithms Sci. Eng.* **2025**, *2025*, 32.

13. Sabit, S.; Souid, M.S.; Benaouda, M.; et al. Fixed Point Analysis for Cauchy-Type Variable-Order Fractional Differential Equations With Finite Delay. *Int. J. Differ. Equ.* **2026**, *2026*, 3615489.
14. Souid, M.S.; Guedim, S.; Boulaaras, S.; et al. New approaches to solving initial value problems of mixed differential equations. *Filomat* **2026**, *40*, 649–659.
15. Bhatter, S.; Jangid, K.; Abidemi, A.; et al. A new fractional mathematical model to study the impact of vaccination on COVID-19 outbreaks. *Decis. Anal. J.* **2023**, *6*, 100156.
16. Gonzalez-Ramirez, L.R. A fractional-order Wilson-Cowan formulation of cortical disinhibition. *J. Comput. Neurosci.* **2024**, *52*, 109–123.
17. Ibrahim, R.W.; Altulea, D.; Elobaid, R.M. Dynamical system of the growth of COVID-19 with controller. *Adv. Differ. Equ.* **2021**, *2021*, 9.
18. Ghanbari, B. *Fractional Calculus: Bridging Theory with Computational and Contemporary Advances*; Elsevier: Amsterdam, The Netherlands, 2024.
19. Xue, D.; Bai, L. *Fractional Calculus: High-Precision Algorithms and Numerical Implementations*; Springer Nature: Berlin/Heidelberg, Germany, 2024.
20. Singh, D.K.; Yavuz, M. *The Fundamentals of Fractional Calculus*; Apple Academic Press: New York, NY, USA, 2025.
21. Atangana, A.; Baleanu, D. New fractional derivatives with nonlocal and non-singular kernel: Theory and application to heat transfer model. *arXiv* **2016**, arXiv:1602.03408.
22. Ibrahim, R.W.; Baleanu, D. Fractional operators on the bounded symmetric domains of the Bergman spaces. *AIMS Math.* **2024**, *9*, 3810–3835.
23. Vats, Y.; Mehra, M.; Oelz, D.; et al. A new perspective for scientific modelling: Sparse reconstruction-based approach for learning time-space fractional differential equations. *J. Comput. Nonlinear Dyn.* **2024**, *19*, 121003.
24. Momani, S.; Baleanu, D.; Ibrahim, R.W. K-Symbol Atangana-Baleanu fractional operators in a complex domain. In Proceedings of the 2023 International Conference on Fractional Differentiation and Its Applications (ICFDA), Ajman, United Arab Emirates, 14–16 March 2023; pp. 1–4.
25. Mohamed, B.G.; Qamlo, A.H. Fractional Optimal Control Problem for Symmetric System Involving Distributed-Order Atangana–Baleanu Derivatives with Non-Singular Kernel. *Symmetry* **2025**, *17*, 417.
26. Althubyani, M.; Saber, S. Hyers–Ulam stability of fractal–fractional computer virus models with the Atangana–Baleanu operator. *Fractal Fract.* **2025**, *9*, 158.
27. Zhang, R.F.; Li, M.C.; Cherraf, A.; et al. The interference wave and the bright and dark soliton for two integro-differential equation by using BNNM. *Nonlinear Dyn.* **2023**, *111*, 8637–8646.
28. Ibrahim, R.W. Differential Operator Associated with the (*q*,k)-Symbol Raina's Function. In *Mathematical Analysis, Differential Equations and Applications*; World Scientific Publishing: Singapore, 2024; pp. 321–342.
29. Ibrahim, R.W.; Baleanu, D. Modified Atangana-Baleanu fractional differential operators. *Proc. Inst. Math. Mech. Natl. Acad. Sci. Az.* **2022**, *48*, 56–67.
30. Attiya, A.A.; Ibrahim, R.W.; Albalahi, A.M.; et al. A differential operator associated with q-Raina function. *Symmetry* **2022**, *14*, 1518.
31. Shao, X.; Lu, Y.; Zhang, J.; et al. Quantized nonfragile state estimation of memristor-based fractional-order neural networks with hybrid time delays subject to sensor saturations. *Fractal Fract.* **2024**, *8*, 343.
32. Aldawish, I.; Ibrahim, R.W. Fractional-order modeling of sediment transport and coastal erosion mitigation in shorelines under extreme climate conditions: A case study in iraq. *Computation* **2025**, *13*, 104.
33. Ibrahim, R.W. A generalized fractional system for modeling climate change and emissions: Analysis, numerical solutions with a case study. *Theor. Appl. Climatol.* **2025**, *156*, 514.
34. Rangasamy, M.; Shalini, M.M.; Dhandapani, P.B.; et al. A neutral stochastic differential system analysis for ABC fractional order with a constant of variations. *Appl. Math. Sci. Eng.* **2025**, *33*, 2438780.
35. World Health Organization (WHO). *Global Health Observatory Data*; WHO: Geneva, Switzerland, 2021.